NASA/TM—2016–219349

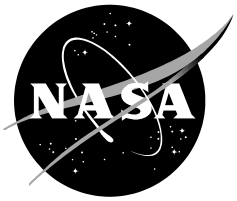

Calculated Low-Speed Steady and Time-Dependent Aerodynamic Derivatives for Several Different Wings Using a Discrete Vortex Method

Donald R. Riley
Langley Research Center, Hampton, Virginia

December 2016

NASA STI Program . . . in Profile

Since its founding, NASA has been dedicated to the advancement of aeronautics and space science. The NASA scientific and technical information (STI) program plays a key part in helping NASA maintain this important role.

The NASA STI program operates under the auspices of the Agency Chief Information Officer. It collects, organizes, provides for archiving, and disseminates NASA's STI. The NASA STI program provides access to the NTRS Registered and its public interface, the NASA Technical Reports Server, thus providing one of the largest collections of aeronautical and space science STI in the world. Results are published in both non-NASA channels and by NASA in the NASA STI Report Series, which includes the following report types:

- TECHNICAL PUBLICATION. Reports of completed research or a major significant phase of research that present the results of NASA Programs and include extensive data or theoretical analysis. Includes compilations of significant scientific and technical data and information deemed to be of continuing reference value. NASA counter-part of peer-reviewed formal professional papers but has less stringent limitations on manuscript length and extent of graphic presentations.

- TECHNICAL MEMORANDUM. Scientific and technical findings that are preliminary or of specialized interest, e.g., quick release reports, working papers, and bibliographies that contain minimal annotation. Does not contain extensive analysis.

- CONTRACTOR REPORT. Scientific and technical findings by NASA-sponsored contractors and grantees.

- CONFERENCE PUBLICATION. Collected papers from scientific and technical conferences, symposia, seminars, or other meetings sponsored or co-sponsored by NASA.

- SPECIAL PUBLICATION. Scientific, technical, or historical information from NASA programs, projects, and missions, often concerned with subjects having substantial public interest.

- TECHNICAL TRANSLATION. English-language translations of foreign scientific and technical material pertinent to NASA's mission.

Specialized services also include organizing and publishing research results, distributing specialized research announcements and feeds, providing information desk and personal search support, and enabling data exchange services.

For more information about the NASA STI program, see the following:

- Access the NASA STI program home page at http://www.sti.nasa.gov

- E-mail your question to help@sti.nasa.gov

- Phone the NASA STI Information Desk at 757-864-9658

- Write to:
  NASA STI Information Desk
  Mail Stop 148
  NASA Langley Research Center
  Hampton, VA 23681-2199

NASA/TM—2016–219349

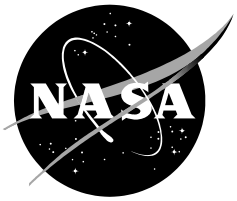

Calculated Low-Speed Steady and Time-Dependent Aerodynamic Derivatives for Several Different Wings Using a Discrete Vortex Method

Donald R. Riley
Langley Research Center, Hampton, Virginia

National Aeronautics and
Space Administration

Langley Research Center
Hampton, VA 23681

December 2016

Acknowledgments

The author would like to thank graphic artist G. Lee Pollard of NCI Information Systems for creating the final figures used in this report.

Available from:

NASA STI Program / Mail Stop 148
NASA Langley Research Center
Hampton, VA 23681-2199
Fax: 757-864-6500

Summary

Calculated numerical values for some aerodynamic terms and stability derivatives for several different wings in unseparated inviscid incompressible flow were made using a discrete vortex method involving a limited number of horseshoe vortices. Both longitudinal and lateral-directional derivatives were calculated for steady conditions as well as for sinusoidal oscillatory motions. Variables included the number of vortices used and the rotation axis/moment center chordwise location. Frequencies considered were limited to the range of interest to vehicle dynamic stability ($k_b < .24$). Comparisons of some calculated numerical results with experimental wind-tunnel measurements were in reasonable agreement in the low angle-of-attack range considering the differences existing between the mathematical representation and experimental wind-tunnel models tested. Of particular interest was the presence of induced drag for the oscillatory condition.

Introduction

An exploratory study was undertaken to calculate numerical values for some aerodynamic terms and stability derivatives for several different airfoils and wings in unseparated inviscid incompressible flow using a discrete vortex method consisting of two-dimensional vortices for airfoils and horseshoe vortices for wings. Calculated values were obtained for both steady conditions and sinusoidal oscillatory motions. Reference 1 provides the study results on two-dimensional airfoils and the present effort presents the information on several different wings. Aerodynamic stability derivatives with respect to angle of attack and sideslip as well as the three angular rates and their time derivatives were calculated herein. For oscillatory motion derivative values were obtained as a function of reduced frequency parameter k_b for the range of interest to vehicle dynamic stability ($k_b < .24$). The purpose of this work was to determine if the use of a limited number of vortices would yield useful numerical values of the various derivatives. The intent of this effort was to make available some comparisons with experimental measurements conducted in wind tunnels at low speed (In particular the experimental data used herein was obtained in the late 1950's following which further research efforts were curtailed and redirected to various tasks required to accomplish the manned lunar landing missions. A comparison of theory with this early experimental data is of interest.).

A large number of theoretical studies of oscillating airfoils and wings exist in the published literature over the past 75 years. (For example see textbooks like reference 2 and numerous NACA/NASA reports, many AIAA journal articles, AGARD publications like reference 3 and many others. The use of indicial functions and advances such as suggested by reference 4 have been employed.) These studies examine the problem for a range of conditions including subsonic and supersonic Mach Numbers as well as for incompressible flow. A large number of mathematical developments for airfoils and wings were limited to their longitudinal lift and moment

characteristics. Less available is oscillatory information on the aerodynamic derivatives due to pitch, roll and yaw angular rates for wings that is of considerable interest at the present time because of the emphasis on tail-less aircraft configurations. Results of the present effort and those of reference 1 provide some additional information.

Symbols

Standard NASA coefficients of forces and moments used herein are referenced to the Wind-Tunnel Stability System of Axes where the origin can be located at various positions on the wing root-chord. Since the calculations for each derivative were made at a given time, different positions of the axis system origin were used and are noted. The positive directions of forces and moments, angles and angular rates are shown in figure 1. The coefficients and symbols are defined as follows:

A aspect ratio

$\bar{A}$ sine wave amplitude

b wing span, *ft*

c airfoil chord, *ft*

c_d airfoil drag coefficient, (drag per unit span)/ $\bar{q}c$

c_l airfoil lift coefficient, (lift per unit span)/ $\bar{q}c$

c_m airfoil pitching moment coefficient, (pitching moment per unit span)/ $\bar{q}c^2$

C_D wing drag coefficient, drag/ $\bar{q}S$

C_L wing lift coefficient, lift/ $\bar{q}S$

C_m wing pitching moment coefficient, pitching moment/ $\bar{q}Sc$

C_l wing rolling moment coefficient, rolling moment/ $\bar{q}Sb$

C_n wing yawing moment coefficient, yawing moment/ $\bar{q}Sb$

C_Y wing side force coefficient, side force/ $\bar{q}S$

d horseshoe vortex semi-span, ft

$F(m,n)$ horseshoe vortex influence coefficient

K_n, k_n individual vortex circulation value, $ft^2 / \sec.$

k_b reduced frequency parameter, $\frac{\omega b}{2V}$

k_c reduced frequency parameter, $\frac{\omega c}{2V}$

N number of horseshoe vortices used

p roll rate, radians/sec.

q pitch rate, radians/sec.

$\bar{q}$ dynamic pressure, $\frac{1}{2}\rho V^2$, lbs/ ft^2

r yaw rate, radians/sec.

S wing area, ft^2

t time, sec.

V free-stream velocity, *ft*/sec.

X_s, Y_s, Z_s wind-tunnel stability axis system

α angle of attack, radians (in degrees where noted)

β angle of sideslip, radians

ω circular angular velocity, radians/sec.

ρ density of air, slugs/ ft^3

$\Lambda_{c/4}$ quarter-chord sweep angle, radians or degrees

Λ_{le} leading-edge sweep angle, radians or degrees

τ taper ratio

ϕ phase angle, radians

Φ indicial function

$$C_{L_\alpha} = \frac{\partial C_L}{\partial \alpha} \quad C_{L_q} = \frac{\partial C_L}{\partial \frac{qc}{2V}} \quad C_{l_p} = \frac{\partial C_l}{\partial \frac{pb}{2V}} \quad C_{l_r} = \frac{\partial C_l}{\partial \frac{rb}{2V}} \quad C_{l_\beta} = \frac{\partial C_l}{\partial \beta}$$

$$C_{L_{\dot\alpha}} = \frac{\partial C_L}{\partial \frac{\dot\alpha c}{2V}} \quad C_{L_{\dot q}} = \frac{\partial C_L}{\partial \frac{\dot q c^2}{(2V)^2}} \quad C_{l_{\dot p}} = \frac{\partial C_l}{\partial \frac{\dot p b^2}{(2V)^2}} \quad C_{l_{\dot r}} = \frac{\partial C_l}{\partial \frac{\dot r b^2}{(2V)^2}} \quad C_{l_{\dot\beta}} = \frac{\partial C_l}{\partial \frac{\dot\beta b}{2V}}$$

Additional derivatives obtained by replacing L with m, and l with n or Y.
A dot over a symbol represents a derivative with respect to time.

Subscripts:

ss steady state conditions

ω oscillatory conditions

Basic Considerations

A number of stability derivatives exist for airfoils and wings for steady and oscillatory conditions. Since numerous comparisons of theory and experimental values for steady conditions have been made in the published literature over the years, the effort here is directed principally toward the oscillatory condition. It should be recognized that the steady condition is, of necessity, examined first in all cases prior to considering oscillatory motion and consequently a few examples are mentioned when they are of interest. Note that for steady conditions, experimental measurement of the stability derivatives for some wings due to constant angular rate in p or q or r were made in the rolling flow and curved flow test sections of the NASA Langley Stability Tunnel in the 1940's and 50's (reference 5).

Theory

The discrete vortex method considers the shape of the airfoil section to be symmetrical. Thus airfoils can be represented by their chords, and wings can be represented by flat-chord planes. For airfoils, the chord is divided into a number of segments. A vortex is located at the quarter-chord of each segment and a control point at the three-quarter-chord position. The velocity generated by the sum of the vortices at the control point is set equal to the external velocity normal to the airfoil surface. Solution of the resulting set of simultaneous equations yields values of the unknown circulations and thus the lift. For airfoil time-dependent -calculations use is made of a starting vortex positioned at a quarter-chord aft of the trailing edge at time equals zero. As time increases vortices are shed downstream in the wake. Calculation of the lift on the airfoil surface at each new wake location yields the response to a step input. From this result the frequency response can be calculated and values for the stability derivatives can be obtained. For wings the time-dependent calculations are similar except that horseshoe vortices are employed. The vortices in the wake effectively result in elongated loops with increasing time. Finally the calculation procedure gives values of the wing stability derivatives as a function of the reduced frequency parameter k_b or k_c .

Wind Tunnel Experimental Measurements

Experimental values were obtained only for the lateral-directional derivatives from tests in the Langley Stability Tunnel on three wings illustrated in figure 2 as reported in references 6, 7, 8,and 9. The tests in reference 6 and7 are believed to be the first attempt to obtain pure oscillatory sideslip and yawing velocity measurements for wings. Each of the three wings was mounted to a two-component strain gage balance at the quarter-chord of the mean aerodynamic chord and measurements were made of

the rolling and yawing moments. Tests were made for an angle of attack range through stall at several values of oscillation frequency. Of interest herein are those tests made at the single frequency designated by k_b = .22 . Canopies were used on all wings to cover the balance that extended above the wing upper surface to prevent airflow through the wing. The tests were conducted at a dynamic pressure of 24.9 lbs. per square foot.

Results And Discussion

Longitudinal Characteristics

Values for steady conditions for the aerodynamic derivatives for several different rectangular wings due to angle of attack and separately due to pitch rate were calculated using horseshoe vortices. These results are given in figure 3 and illustrate the influence of wing aspect ratio. The pitch rate derivatives were first presented by Glauert in reference 10 published in 1928 and give values (converted herein to NASA nomenclature) comparable to but with magnitudes slightly greater than those shown. Worth noting is the symmetry of the moment derivative values about the mid-chord position.

As an initial attempt at examining oscillating three dimensional wings, calculations were made to obtain the lift derivatives due to angle of attack for an aspect ratio 4 rectangular wing using a single horseshoe vortex spanning the wing as shown in figure 4. A starting horseshoe vortex with the same value of circulation but opposite rotation is placed at $c/4$ aft of the wing trailing edge. The trailing vortices downstream cancel and thus the resulting vortex system in the wake forms elongated rectangular loops as the wake moves downstream. Figure 5 shows the lift indicial function and figure 6 gives the resulting numerical values for the derivatives C_{L_α} and $C_{L_{\dot{\alpha}}}$ as a function of k_c. Figure 7 shows the induced drag function with increasing time and figure 8 illustrates two example induced drag-displacement traces for different oscillation frequencies obtained in a manner similar to that used in reference 1. Figure 9 shows the corresponding lift –displacement trace when k_c = .05. These results using a single horseshoe vortex were part of a number of calculations varying the number of horseshoe vortices chordwise and spanwise. They are presented here because they are the only longitudinal case for which induced drag information was calculated. It is recognized that derivative magnitudes predicted using a single horseshoe vortex exceed those of comparable experimental measurement. To provide an example of the pitch-rate derivatives, figure 10 shows two arrangements using four horseshoe vortices equally spaced across the chord for both the 2-D airfoil and the aspect ratio 4 wing. Figures 11 and 12 give the lift and moment values of the indicial functions for both the initial and terminal conditions. The difference in the curves is an indication of the time dependency involved. Figure 12 shows the skewed shape of the pitching moment curves obtained at the starting condition for both the 2-D airfoil and

aspect ratio 4 wing. Finally, to obtain realistic values for the oscillatory lift derivatives for the aspect ratio 4 wing, figure 13 gives values for lift derivatives due to α using eight horseshoe vortices spanning the wing. The associated oscillatory lift derivatives due to pitch-rate and the summed combination are given in figures 15, 16 and 17. Two rows of horseshoe vortices (figure14) were used to give an improved pitch-rate effect. Figure 18 presents a comparison of the results of the aspect ratio 4 wing with the two-dimensional case illustrating the large reduction in the magnitude of the derivative values due to three-dimensional effects and the loss in frequency dependence.

Jones in reference 11 presented the indicial lift function for a sudden change in angle of attack for elliptical wings of aspect ratio 3 and 6. Figure 19 presents his result given by equation 29 of reference 11 in the notation used in this paper. Note that the abscissa variable is the distance traveled in root-semi-chords of the elliptical planform. Also shown for comparison with the results of these two wings is Wagner's result for a two-dimensional airfoil given by equation 30 of reference 11 and by equation (5-371) of reference 2. This curve was included to illustrate how quickly the lift of the elliptical wing approaches the steady state limit as compared to that of the two-dimensional airfoil. The few additional data points on the figure are for the rectangular wing of aspect ratio 4 calculated herein. The ordinate values for the data were plotted at adjusted abscissa values using the relation

$$\frac{\pi}{4}\frac{Vt}{c/2} = \frac{Vt}{c_r/2}$$

where c is the rectangular wing chord, and
c_r is the elliptical wing root chord

so that the wake position relative to the wing trailing edge was more compatible with that of the elliptical wing. (See Appendix A) The comparisons of results shown on figure 19 and 20 for the rectangular and the elliptical wings are in good agreement thus serving as a check on the computational procedure.

Lateral-Directional Characteristics

Roll-Rate Derivatives

Calculations to obtain the rolling-moment stability derivatives due to roll rate for a rectangular wing of aspect ratio 8 were made for the wing centerline chord aligned with the relative wind. For this situation the wing angle of attack is zero and the wing rolls about the velocity vector. To calculate the oscillatory stability derivatives, a step input is applied in roll rate and as time increases vortices are shed downstream in the wake. The wing-tip helix angle is assumed small so that the wake cross-section roll attitude can be neglected in the calculations. Figure 21 shows the load distribution at the initiation and termination of the step input depicted using 12 horseshoe vortices placed spanwise to represent the wing. The area located between

the curves represent, of course, the time dependent portion of the derivatives. Figure 22 gives the indicial function for the rolling moment calculated herein and figure 23 gives the frequency response values for the stability derivatives C_{l_p} and $C_{l_{\dot{p}}}$ as a function of the reduced frequency parameter k_b. The results show the derivative magnitudes change very slightly over the frequency range shown. Figure 24 gives a rolling-moment versus displacement trace and figure 25 gives an estimate of the corresponding induced-drag--parameter versus rate-displacement trace using eight horseshoe vortices to represent the wing. The latter result indicates that a time history of the drag force would show it oscillates at twice the oscillation frequency. (For drag development see reference 1.) In addition there exists a profile drag component that must be considered when comparing these results with experimental measurements. With the centerline chord set at $\alpha = 0^o$ the side force and yawing moment are both zero. If an angle of attack is introduced the derivatives C_{n_p} and C_{y_p} also their time derivatives can acquire values particularly for tapered and swept wings. Additional time dependent calculations were not attempted since experimental wind-tunnel measurements were not available.

Yaw-Rate Derivatives

Calculations to obtain the oscillatory stability derivatives due to yaw rate were made for a rectangular wing of aspect ratio 8 with the origin of the Stability Axis System located at the quarter-chord of the root chord. For the wing operating at zero angle of attack and yawing about the Z stability axis, only profile drag forces occur. Integrating these forces across the wing span gives a value of C_{n_r} of $-\frac{1}{3}c_d$. The corresponding rolling moment and side force derivatives C_{l_r} and C_{Y_r} are of course zero. If the wing is set at a small angle of attack then lift is developed and values of all of the yaw-rate derivatives can be calculated. Figure 26 gives the rolling moment time response due to a step input in yaw rate and some of the equations involved are given in Appendix B. As in the case of the roll-rate derivatives, the yaw-rate derivatives show very little variation with k_b over the frequency range $0 \geq k_b \geq .24$. Numerical values obtained for the rolling-moment due to yaw-rate derivatives at $k_b = .22$ were $\left(C_{l_r}\right)_\omega = .4352\pi\alpha$ and $\left(C_{l_{\dot{r}}}\right)_\omega = -.0113\pi\alpha$. Calculations were not made for the corresponding time-dependent yawing moment and side force derivatives however steady state values were computed. These derivative values compared very well with published results in references 12,13 and 14 as shown in Table 1.

Experimental wind-tunnel measurements for the stability derivatives due to pure yaw-rate are available in reference 7 for a single oscillation frequency ($k_b = .22$) for three wings: a 60^o delta, a 45^o sweptback, and an unswept wing (see figure 2). Figure 27 shows a schematic sketch of the oscillating apparatus and figure 28 shows the three wings mounted on the oscillation apparatus in the Langley Stability Tunnel.

As shown in figure 2 the moment center and rotation axis is located at the quarter-chord of the mean aerodynamic chord. From consideration of the effect of shed vortices in the wake and from previous experience from reference 1 and the previous section herein, an indicial function was established and the steady stability derivative $\left(C_{l_r}\right)_{ss}$, and the oscillatory derivatives $\left(C_{l_r}\right)_{\omega}$ and $\left(C_{l_{\dot{r}}}\right)_{\omega}$ were calculated for $k_b = .22$. A similar indicial function was used along with the steady-state yawing-moment derivative $\left(C_{n_r}\right)_{ss}$ and its value at time equals zero to obtain values for the yawing moment derivatives at $k_b = .22$. Numerical values calculated for both derivatives were obtained in terms of angle of attack. These values were modified by the ratio of steady-state lift-cure slopes (experimental to vortex calculated) and the results compared with wind-tunnel measurements given in reference 7.
Figures 29a, 29b, 29c and figures 30 and 31 present the data of reference 7 with the modified values calculated herein overlaid to provide a direct comparison of theory and experimental results. As presented, a comparison shows reasonable agreement in the low and medium angle of attack range. Although some differences are apparent at the low angles of attack, some are quite large at the higher angles of attack. The corresponding numerical values calculated for the derivatives are given in Tables 2 and 3.

Sideslip Derivatives

Calculations for several wing planforms using different numbers of horseshoe vortices were made initially to obtain values for the rolling-moment derivative due to sideslip, C_{l_β}, for steady flow conditions. During this process it was noticed that by using only two horseshoe vortices to represent wings having straight leading and trailing edges, equations for the sideslip parameters $\frac{C_{l_\beta}}{C_L}$ and $\frac{C_{n_\beta}}{(C_L)^2}$ could be developed yielding numerical values comparable to those in reference 15 for $\frac{C_{l_\beta}}{C_L}$ without the Weissinger correction factor of +.05 applied. These equations are given in Appendix C. Calculations for the three different wings were made initially to obtain values for the rolling moment derivative due to sideslip for steady flow conditions using N=2. Calculations were also made for the starting condition. Using these two results in conjunction with information for a number of downstream stations, an indicial function was established (figure 32) and values for the oscillatory derivatives $\left(C_{l_\beta}\right)_{\omega}$ and $\left(C_{l_{\dot{\beta}}}\right)_{\omega}$ for each wing were obtained for $k_b = .22$. These results are presented in Table 2. Corresponding values for the oscillating yawing moment derivatives were obtained using calculated values for the steady state parameter

$\left(C_{n_\beta}\right)_{ss}$ in conjunction with the indicial function obtained in a manner similar to the rolling moment derivative. This approach was used since the yawing moment results from tilt of the force on the trailing leg vortex segments due to angle of attack. These results are given in Table 3. The theory values for each sideslip derivative listed in Tables 2 and 3 have been modified by the lift-curve slopes ratio (experimental to calculated theory) to permit a direct comparison of experimental and theoretical results. Figures 33 thru 36 present a comparison of calculated derivative values with the experimental measurements taken from figures 19, 20, 21, and 22 of reference 9. It is worth noting that the original sideslip forced oscillation tests for the three wings was reported in reference 8. These tests were repeated for the single frequency $k_b = .22$ in reference 9 to more nearly match the pure yawing oscillation test conditions mentioned earlier. Lastly, figures 33 thru 36 present a comparison of calculated and experimental values of the oscillatory sideslip derivatives as a function of angle of attack. An examination of the data indicates that the calculated values reasonably estimate the magnitudes of the derivatives at low angles of attack. Some difference was expected since the Weissinger correction factor of deflecting the wake trailing vortices at the wing trailing edge through the sideslip angle was not included in the calculations. Incorporating this effect should improve the comparisons presented. The largest difference between results of experiment and theory occurs for the 45^o swept wing. The difference originates at a low angle of attack ($\alpha = 4^o$) and increases as angle of attack is increased. The effect is believed to be due to the leading edge vortices lateral movement over the wing upper surface with angle of attack.

Derivative Combinations

Reference 9 presents wind-tunnel measurements of the rolling-moment and yawing-moment stability derivatives for the same three wings shown in figure 2 performing sinusoidal oscillation in yaw about a vertical wind axis (see figure 37). Photographs of the wings mounted in the wind tunnel are given in figure 39. The aerodynamics from this motion arise from the combination of sideslip and yaw rate. The stability derivatives thus obtained are in combination form as (see Appendix D):

$$C_{l_r} - C_{l_{\dot\beta}},\ C_{l_\beta} + k_b^2 C_{l_{\dot r}},\ C_{n_r} - C_{n_{\dot\beta}},\ C_{n_r} + k_b^2 C_{n_{\dot r}}$$

In order to calculate values of the combination derivatives, it is necessary to calculate the sideslip β and yaw-rate r contributions separately. These contributions for the single frequency $k_b = .22$ are given in the preceding sections and the final values were obtained for the combination derivatives. These values are given in Tables 2 and 3. A graphical comparison of these calculated values with experimental measurements of reference 9 is given in figures 40 through 43 by simply plotting the values for the calculated curves on copies of the data points and curves from figures 19 through 22 of reference 9. The data points (circles) are the measured values from the oscillation in yaw test and the solid lines are the summed data values from the component

experimental measurement tests. Comparison of the calculated curves (dashed lines) with the circular data points indicates reasonable agreement at low angles of attack for all three wings. The large difference between theory and experiment for the rolling moment derivative for the 45^o swept wing above $\alpha = 4^o$ occurs because of the inability of the theory to correctly predict values for the sideslip component. An exact comparison between theory and experiment should not be expected for any of the three wings not only because of the assumptions made in the math model but also because of differences that exist between the mathematical representation used for the calculations and the actual model tested (see Table 4). Nevertheless, the comparisons shown indicate that at low angles of attack vortex theory predicts acceptable numerical values for these particular derivatives (a discussion comparing the experimental data points with the added experimental measured components is presented in reference 9).

Concluding Remarks

An exploratory study was undertaken to calculate numerical values for some aerodynamic terms and stability derivatives for several different wings in unseparated inviscid incompressible flow using a discrete vortex method involving a limited number of vortices. Both longitudinal and lateral-directional derivatives were calculated for steady conditions and also for sinusoidal oscillatory motions. Frequencies considered were limited to the range of interest to vehicle dynamic stability $k_b < .24$. Comparison of some calculated results with experimental wind-tunnel measurements were in reasonable agreement in the low angle of attack range considering the differences in the mathematical representation and experimental wind-tunnel model tested. For the frequency range considered, the magnitudes of the stability derivatives for wings decrease with increasing frequency. Equations were developed for sideslip derivatives for wings having straight leading and trailing edges in steady flow that were in agreement with previously published information. Of particular interest was the presence of induced drag for the oscillating condition due to the vortices shed in the wake interacting with those representing the wing surface. The number of horseshoe vortices was varied for calculating values for the different derivatives considered. For some derivatives such as C_{L_α} and C_{l_p} more horseshoe vortices were used to obtain a better definition of the load distribution. For derivatives that were calculated in parameter form such as $\frac{C_{l_r}}{C_L}$ and $\frac{C_{l_\beta}}{C_L}$ only several vortices were needed since both numerator and denominator values varied with the number of horseshoes chosen.

Appendix A

Wake Displacement Adjustment

Jones in reference 11 (published in 1940) provided values of the lift indicial function due to a step input in angle of attack for two elliptical wings as a function of downstream distance traveled by the wake in terms of the root-semi-chord of the elliptical wing. In order to compare the indicial function of rectangular aspect ratio 4 wing with the elliptical wing indicial function an adjustment to the wake downstream spacing is required. The relationship between the chords of an elliptical wing and a rectangular wing of equal area can be obtained thusly:

Area of an elliptical wing, $S = \pi \frac{c_r}{2} \frac{b}{2}$

Area of a rectangular wing, $S = cb$

For equal areas, $cb = \frac{\pi}{4} c_r b$

For wings of equal span, then $c = \frac{\pi}{4} c_r$

Adjusting the spacing of the rectangular wing to match that of the elliptical wing yields the comparison given in figure 19. An alternate way to obtain a comparison is to substitute the chord relationship into the equation of the Jones indicial functions as was done in figure 20. Jones equations are:

A=3: $\Phi_{L\alpha} = 0.600\left\{1.000 - .283e^{-.540\frac{Vt}{c_r/2}}\right\}$

A=6: $\Phi_{L\alpha} = 0.740\left\{1.000 - .361e^{-.381\frac{Vt}{c_r/2}}\right\}$

Substituting the chord relationship by replacing c_r by $\frac{4}{\pi} c$ yields:

A=3: $\Phi_{L\alpha} = .600 - .1698e^{-.4241\frac{Vt}{c/2}}$

A=6: $\Phi_{L\alpha} = .740 - .26714e^{-.2992\frac{Vt}{c/2}}$

Figure 20 presents the indicial function comparison based on the rectangular wing chord.

Appendix B

Equations Used For Determining Yaw-Rate Derivatives

A rectangular wing operating at zero angle of attack and oscillating in yaw experiences only profile drag forces and a resulting yawing moment.
If the wing is set at a small angle of attack, then lift is developed. The basic matrix equation for determining the velocity normal to the surface at the control point due to the horseshoe vortex arrangement representing the wing is:

$$\left[w_m\right] = \left[F_{mn}\right]\left[\frac{k_n}{4\pi d}\right] \qquad (1)$$

where subscript m specifies a given control point, n a given horseshoe vortex, and $\left[F_{mn}\right]$ is a square matrix.

Since the velocity across the wing span varies with yaw rate, then the scalar equation that satisfies the condition of no flow thru the wing surface at any specific control point can be written as:

$$w_m - \left(V - ry_m\right)\alpha = 0 \qquad (2)$$

Expressed in matrix form, the problem can be divided into two parts yielding two sets of circulation values, thusly:

Part A $$\left[V\alpha\right] = \left[F_{mn}\right]\left[\frac{k_n}{4\pi d}\right] \qquad (3)$$

Part B $$\left[-ry_m\alpha\right] = \left[F_{mn}\right]\left[\frac{k_n}{4\pi d}\right] \qquad (4)$$

The expression for Part A is the form used to determine the circulation values for angle of attack. The expression for Part B can be written as:

$$\left[-\frac{y_m}{b/2}\right] = \left[F_{mn}\right]\left[\frac{k_n}{4\pi d\alpha rb/2}\right] \qquad (5)$$

Equation 5 can be solved for the values of k_n for Part B in the standard way by multiplying both sides by the inverse of $\left[F_{mn}\right]$.

To compute the rolling moment use is made of the Kutta-Joukowski equation for lift. The rolling moment can be written as:

$$l = \sum_1^n -\rho\left(V - ry_n\right)\left(k_n y_n\right)2d \qquad (6)$$

Where the load for each horseshoe vortex is considered concentrated at the center of each horseshoe vortex and y_n is the spanwise distance from the yaw axis to the center of a bound vortex.

Equation 6 can be rewritten as:

$$l = \sum_1^n -\rho V\left(1 - \frac{rb}{2V}\frac{y_n}{b/2}\right)\left(k_n y_n\right)2d \qquad (7)$$

Equation 7 is applied to the values of k_n of both Part A and Part B. An additional rolling moment contribution, Part C, arises from the presence of the spanwise component of the yawing velocity interacting with the circulation values of the horseshoe vortex trailing legs of Part A. Finally, summation of Parts A, B, and C can be converted to derivative form. Side force and yawing moment derivatives due to yaw rate arise from interactions of velocities and circulations of the various horseshoe vortex segments.

Appendix C

Some Steady Sideslip Derivative Equations

Values for steady sideslip stability derivatives in unseparated inviscid incompressible flow were calculated for a number of thin flat wings having straight-line leading and trailing edges for different values of aspect ratio, taper ratio, and sweep angle. The equations developed for $\frac{C_{l_\beta}}{C_L}$ and $\frac{C_{n_\beta}}{C_L{}^2}$ using 2 horseshoe vortices were obtained as:

$$\frac{C_{l_\beta}}{C_L} = -\left[\frac{3}{2A}\left(\frac{\tau}{\tau+1}\right)+\frac{1}{4}\tan\Lambda_{c/4}\right]$$

$$\frac{C_{n_\beta}}{C_L^2} = \left[\frac{3}{2A}\left(\frac{\tau}{\tau+1}\right)+\frac{1}{4}\tan\Lambda_{c/4}\right]\frac{1}{2\pi A}\left[2.2365+.8038A+.0117A^2\right]$$

These equations apply for various aspect ratios up to 10, taper ratios from 0 to values greater than 1.0, and for both swept-back and sweep-forward semi-spans. Note that these equations neglect the small contributions due to the change in circulation by deflecting the wake and the moment increments due to the side force.

An estimate of the side-force derivative for unswept and swept-back tapered planforms using two horseshoe vortices was obtained as:

$$\frac{C_{Y_\beta}}{C_L{}^2} = -\frac{5}{4\pi A}$$

This expression was obtained by combining the lateral component of the drag force at sideslip in the stability axis system with the side force induced on the wing chordwise vortices from deflecting the wake through the sideslip angle (for forward swept wings, numerical values require calculations using more horseshoe vortices for the latter contribution and values less than those given by the equation were obtained).

Standard NASA coefficients of forces and moments are used that are referenced to the wind-tunnel stability system of axes with the origin located on the wing root chord. For the vortex arrangements with N=2, the location of the origin differs for the different planforms and its location aft of the root-chord leading edge is given by

$$x = \frac{c_r}{4}\left[1+A\left(\frac{1+\tau}{2}\right)\tan\Lambda_{c/4}\right]$$

The positive directions, moments, and angles are shown in figure 1. Note that for the data herein, transfer equations were used to shift the origin to the quarter-chord of the mean aerodynamic chord of each wing.

Appendix D

Wind-Tunnel Measurement

Consider a thin wing in a wind tunnel performing sinusoidal oscillations in yaw about the vertical wind axis (stability axis). Assume the airstream is horizontal and parallel to the wind tunnel centerline. If ψ designates the yaw angle of the wing about the vertical axis measured relative to the wind tunnel centerline, the following equations apply:

$$\psi = \psi_o \sin \omega t$$
$$\dot{\psi} = \psi_o \omega \cos \omega t$$
$$\ddot{\psi} = -\psi_o \omega^2 \sin \omega t$$

where ψ is the instantaneous yaw angle at any time t and ψ_o is the amplitude of the motion. The aerodynamic rolling moment about the longitudinal stability axis can be written as:

$$C_l = C_{l_\beta}\beta + C_{l_{\dot{\beta}}}\frac{\dot{\beta}b}{2V} + C_{l_r}\frac{rb}{2V} + C_{l_{\dot{r}}}\frac{\dot{r}b^2}{4V^2}$$

Recognizing that

$$\beta = -\psi \qquad r = \dot{\psi}$$
$$\dot{\beta} = -\ddot{\psi} \qquad \dot{r} = \ddot{\psi}$$

Upon proper substitution yields the following:

$$\frac{\dot{\beta}b}{2V} = \frac{\left(-\dot{\psi}\right)b}{2V} = \left(\frac{-rb}{2V}\right)$$

and

$$\frac{\dot{r}b^2}{4V^2} = \frac{\ddot{\psi}b^2}{4V^2} = -\psi_o \omega^2 \sin \omega t \left(\frac{b}{2V}\right)^2$$
$$= -\psi_o k^2 \sin \omega t$$
$$= -\psi k^2 = \beta k^2$$

Replacing these two terms in the moment equation gives

$$C_l = (C_{l_\beta} + k_b^2 C_{l_{\dot{r}}})\beta + (C_{l_r} - C_{l_{\dot{\beta}}})\frac{rb}{2V}$$

Each aerodynamic term of this equation can be a function of motion amplitude and reduced frequency. The first term is in-phase with the angular displacement ψ and the second term is out-of-phase with ψ. Analogous development can be made for yawing moment and side force derivatives. The main assumption in the above development is that there is no coupling between the β and r contributions.

References

1. Riley, Donald R.: Calculated Low-Speed Steady And Time Dependent Aerodynamic Derivatives For Some Airfoils Using A Discrete Vortex Method, NASA TM -2015-218998
2. Bisplinghoff, Raymond L.; Ashley, Holt; Halfman, Robert L.: Aeroelasticity, Addison-Wesley Publishing Company Inc., 1955
3. Special Course on Unsteady Aerodynamics; AGARD REPORT 679, March 1980
4. Tobak, Murray and Schiff, Lewis B.: On The Formulation Of The Aerodynamic Characteristics In Aircraft Dynamics NASA TR R-456, 1976
5. Baals, Donald D. and Corliss, William R.: Wind Tunnels of NASA; NASA SP 440, 1981, p. 43
6. Riley, Donald R.; Bird, John D. and Fisher, Lewis R.: Experimental Determination Of The Aerodynamic Derivatives Arising From Acceleration In Sideslip For A Triangular, A Swept And An Unswept Wing, NACA R M L55A07, 1955
7. Queijo, M.J.; Fletcher, Herman S.; Marple, C. G.; and Hughes, F. M.: Preliminary Measurement Of The Aerodynamic Yawing Derivatives Of A Triangular, A Swept, And An Unswept Wing Performing Pure Yawing Oscillations With A Description Of The Instrumentation Employed. NACA RM L55L14, 1956
8. Lichtenstein, Jacob H. and Williams James L.: Low-Speed Investigation Of The Effects Of Frequency And Amplitude Of Oscillation In Sideslip On The Lateral Stability Derivatives For A 60^o Delta Wing, A 45^o Sweptback Wing, And An Unswept Wing. NACA RM L58B26, 1958
9. Fisher, Lewis R.: Experimental Determination Of Effects Of Frequency and Amplitude On The Lateral Stability Derivatives For A Delta. A Swept, and an Unswept Wing Oscillating In Yaw, NACA TR 1357, 1958
10. Glauert, H.: The Lift And Pitching Moment Of An Airfoil Due To Uniform Angular Velocity In Pitch, R&M No. 1216, British A.R.C., 1928
11. Jones, Robert T.: The Unsteady Lift Of A Wing Of Finite Aspect Ratio; NACA TR 681, 1940
12. Etkin, Bernard: Dynamics of Flight – Stability And Control; Second Edition; John Wiley & Sons, 1982
13. Toll, Thomas A. and Queijo, M. J.: Approximate Relations And Charts For Low-Speed Stability Derivatives Of Swept Wings; NACA TN 1581, 1948
14. USAF Stability and Control Datcom, McDonnell Douglas Corp., Oct. 1960 (Revised Apr. 1976)
15. Queijo, M.J.: Theoretical Span Load Distributions And Rolling Moments For Sideslipping Wings Of Arbitrary Planform In Incompressible Flow, NACA TR 1269, 1956

Table 1. Directional Derivatives For Steady Conditions

Source	$\frac{C_{l_r}}{C_L}$	$\frac{C_{l_\beta}}{C_L}$	$\frac{(\Delta C_{n_r})_1}{C_L{}^2}$	$\frac{(\Delta C_{n_r})_2}{C_{D_o}}$	$\frac{C_{y_r}}{C_L{}^2}$
Etkin, Ref 12	.270	-.040	-.01	-.30	_____
Toll & Queijo, Ref 13	.265	_____	-.019	-.30	0
Datcom, Ref 14	.280	_____	-.019	-.30	_____
Calculated Herein	.280	_____	-.0151	$-\frac{1}{3}$	0

Table 2. Summary Of Rolling Moment Derivative Values For Three Wings

Values for individual components, combined derivatives, and comparison of the latter with experimental measurements for k_b = .22 (angle-of-attack in degrees)

Wing Sweep Deg.	$c_{l_{r,\omega}}$	$c_{l_{\dot{r},\omega}}$
60	$.0143\alpha$	$-.0091\alpha$
45	$.0216\alpha$	$-.0365\alpha$
0	$.0152\alpha$	$-.0141\alpha$
Wing Sweep Deg.	$c_{l_{\beta,\omega}}$	$c_{l_{\dot{\beta},\omega}}$
60	$-.0104\alpha$	$-.0019\alpha$
45	$-.0223\alpha$	$-.0045\alpha$
0	$-.0086\alpha$	$-.0017\alpha$
Wing Sweep Deg.	$c_{l_{r,\omega}} - c_{l_{\dot{\beta},\omega}}$	$c_{l_{\beta,\omega}} + k_b^2 c_{l_{\dot{r},\omega}}$
60	$.0163\alpha$	$-.0109\alpha$
45	$.0261\alpha$	$-.0241\alpha$
0	$.0169\alpha$	$-.0092\alpha$
	Experimental	Fisher (Ref. 9)
Wing Sweep Deg.	$c_{l_{r,\omega}} - c_{l_{\dot{\beta},\omega}}$	$c_{l_{\beta,\omega}} + k_b^2 c_{l_{\dot{r},\omega}}$
60	$.0182\alpha$	$-.0107\alpha$
45	$.0287\alpha$	$-.0175\alpha$
0	$.0125\alpha$	$-.0069\alpha$

Table 3. Summary Of Yawing Moment Derivative Values For Three Wings

Values for individual components, combined derivatives, and comparison of the latter with experimental measurements for k_b = .22 (angle-of-attack in degrees)

Wing Sweep Deg.	$c_{n_{r,\omega}}$	$c_{n_{\dot{r},\omega}}$
60	$-.000086\alpha^2$	$.000071\alpha^2$
45	$.000029\alpha^2$	$-.000051\alpha^2$
0	$-.000111\alpha^2$	$.000102\alpha^2$
Wing Sweep Deg.	$c_{n_{\beta,\omega}}$	$c_{n_{\dot{\beta},\omega}}$
60	$.000328\alpha^2$	$.000142\alpha^2$
45	$.000388\alpha^2$	$.000312\alpha^2$
0	$.000263\alpha^2$	$.000211\alpha^2$
Wing Sweep Deg.	$c_{n_{r,\omega}} - c_{n_{\dot{\beta},\omega}}$	$c_{n_{\beta,\omega}} + k_b^2 c_{n_{\dot{r},\omega}}$
60	$-.000229\alpha^2$	$.000331\alpha^2$
45	$-.000282\alpha^2$	$.000385\alpha^2$
0	$-.000321\alpha^2$	$.000267\alpha^2$
	Experimental	Fisher (Ref. 9)
Wing Sweep Deg.	$c_{n_{r,\omega}} - c_{n_{\dot{\beta},\omega}}$	$c_{n_{\beta,\omega}} + k_b^2 c_{n_{\dot{r},\omega}}$
60	$-.000312\alpha^2$	$.000276\alpha^2$
45	$-.000281\alpha^2$	$.000181\alpha^2$
0	$-.000312\alpha^2$	$.000129\alpha^2$

Table 4. Some differences between calculated math-model representation and experimental test measurement

ITEM	ANALYTICAL CALCULATION	EXPERIMENTAL MEASUREMENT
Motion	Sinusoidal	The three individual oscillatory motions consist of yaw-rate, sideslip, and yawing closely approximate a sinusoid –but were not exact.
Environment	Free-air No canopies	Effect of jet-boundary conditions, blockage, and support interference were unaccounted for. Canopies attached.
Output	Mathematical	Heavily damped direct current meter used to establish a mean value of oscillating meter reading visually

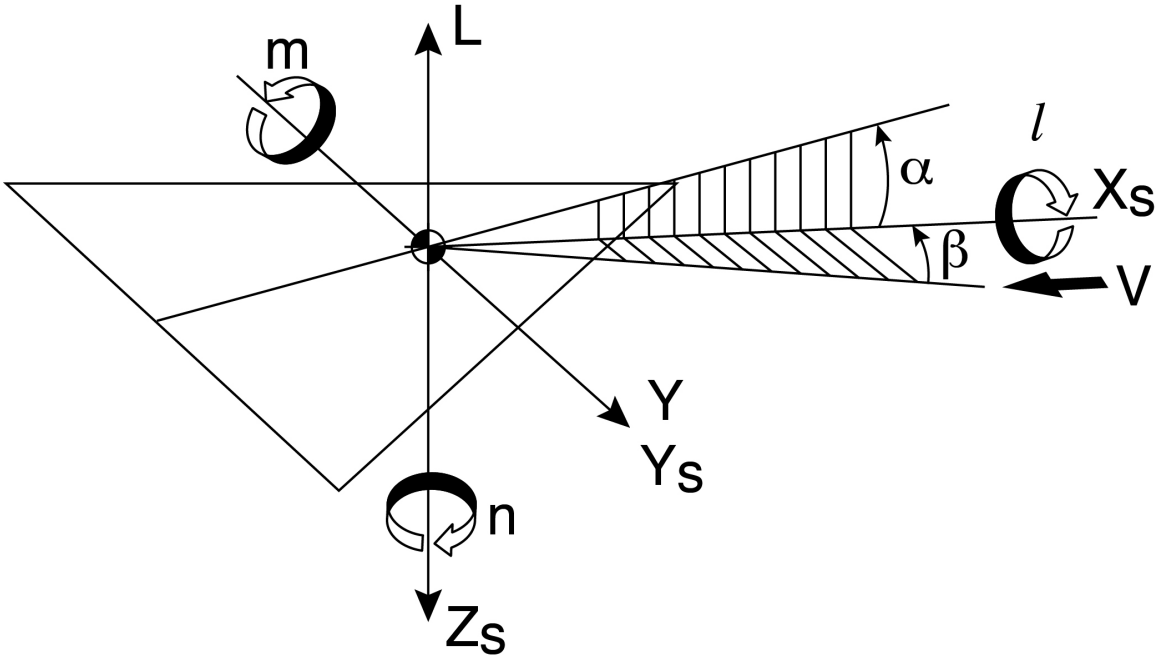

Figure 1. Sketch of axes used (arrows indicate positive directions of forces, moments, and angles)

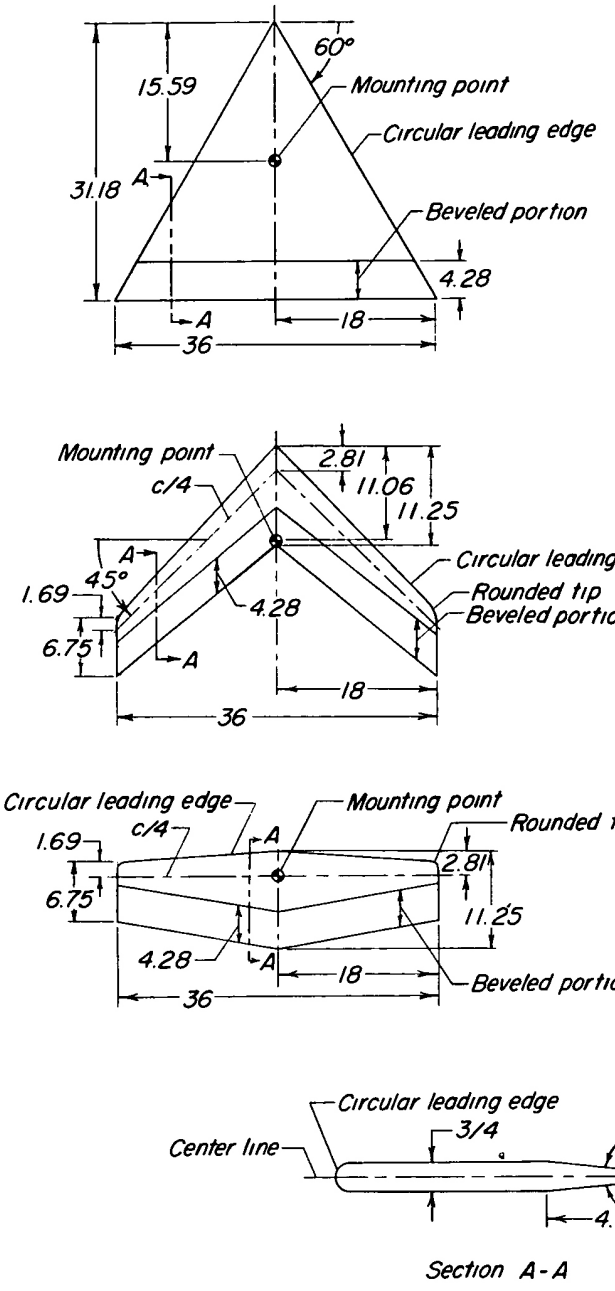

Delta wing

Aspect ratio	2.31
Leading-edge sweep angle, deg	60
Dihedral angle, deg	0
Twist, deg	0
Airfoil section	Flat plate
Area, sq. in.	561.20
Span, in.	36.00
Mean aerodynamic chord, in.	20.79

Swept wing

Aspect ratio	4.0
Taper ratio	0.6
Quarter-chord sweep angle, deg	45
Dihedral angle, deg	0
Twist, deg	0
Airfoil section	Flat plate
Area, sq. in.	324
Span, in.	36
Mean aerodynamic chord, in.	9.19

Unswept wing

Aspect ratio	4.0
Taper ratio	0.6
Quarter-chord sweep angle, deg	0
Dihedral angle, deg	0
Twist, deg	0
Airfoil section	Flat plate
Area, sq. in.	324
Span, in.	36
Mean aerodynamic chord, in.	9.19

Figure 2. Sketches and geometric characteristics of the three wing models investigated (all dimensions are in inches)

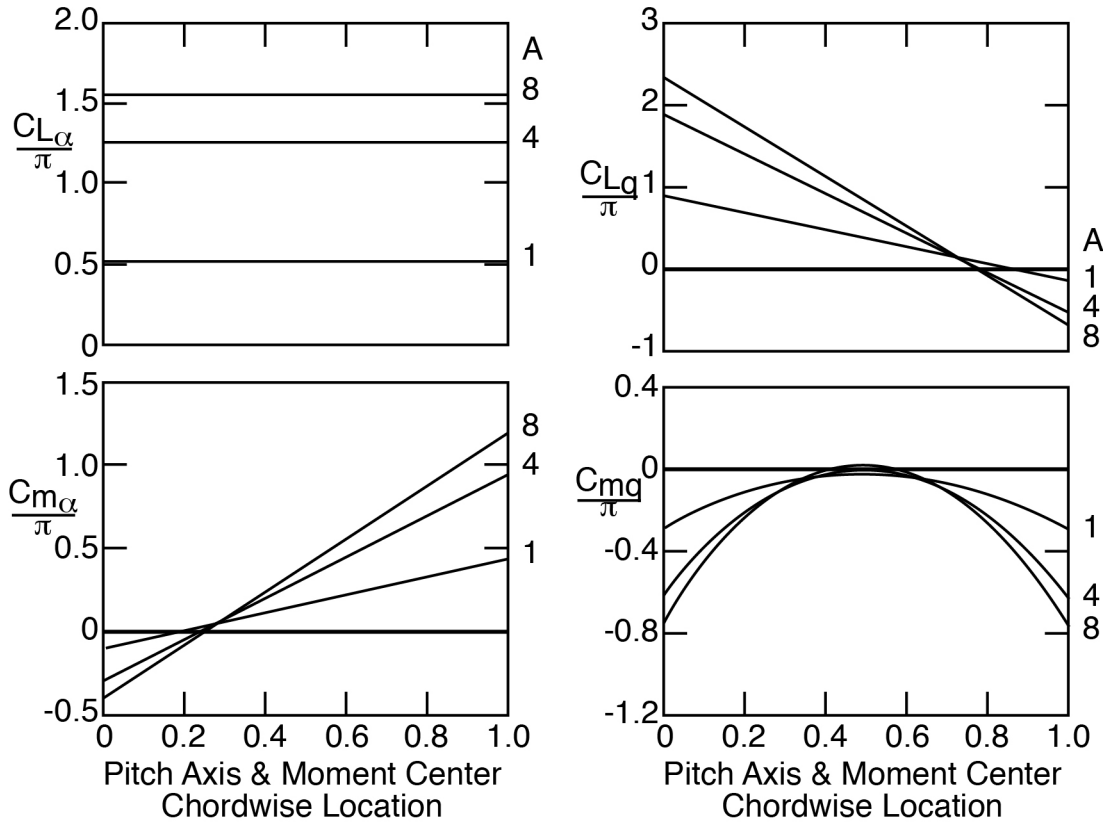

Figure 3. Calculated aerodynamic derivatives for rectangular wings using the discrete horseshoe vortex method with two rows of eight spanwise horseshoe vortices

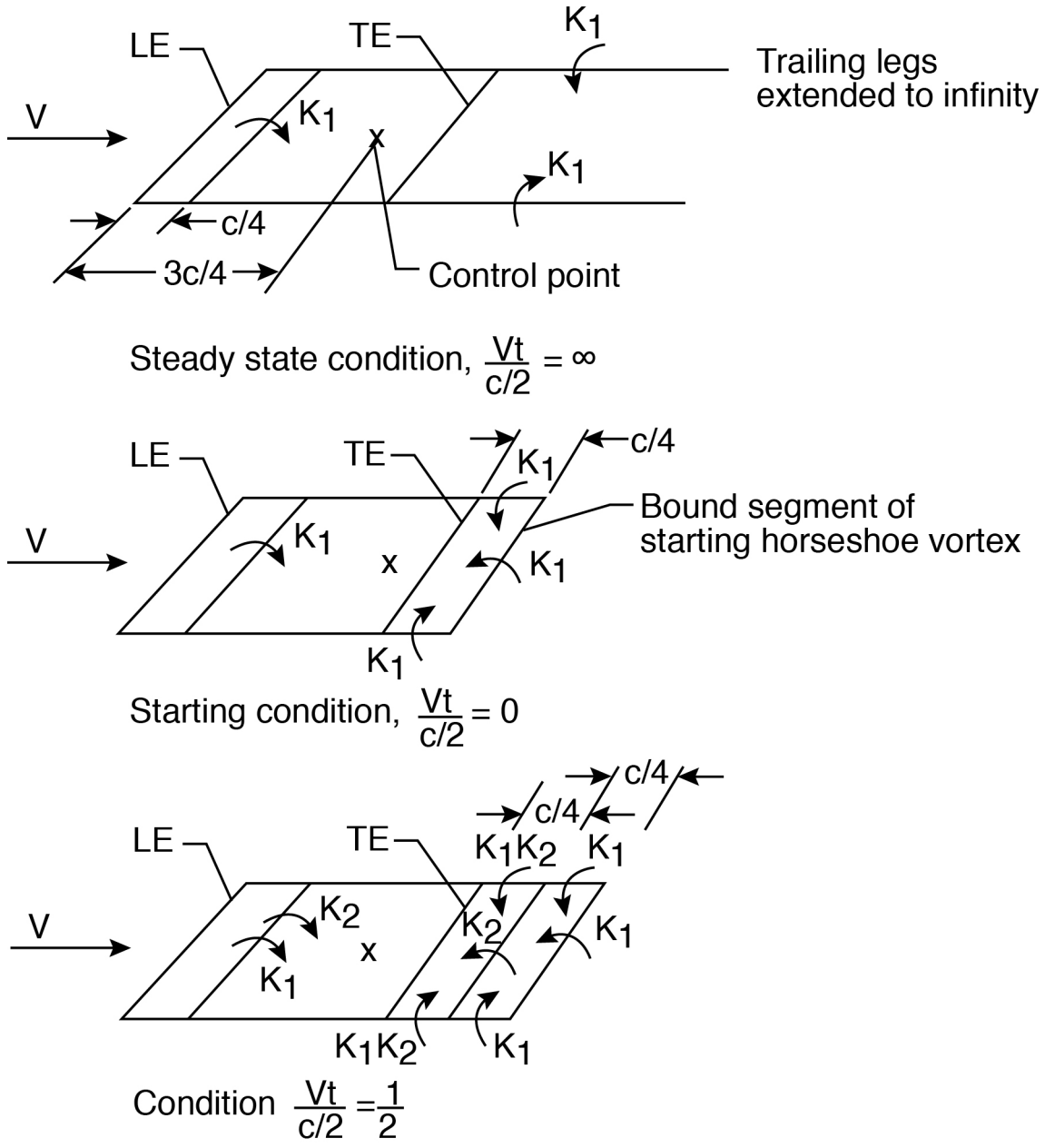

Figure 4. Sketches for a single horseshoe vortex representation showing wake progression

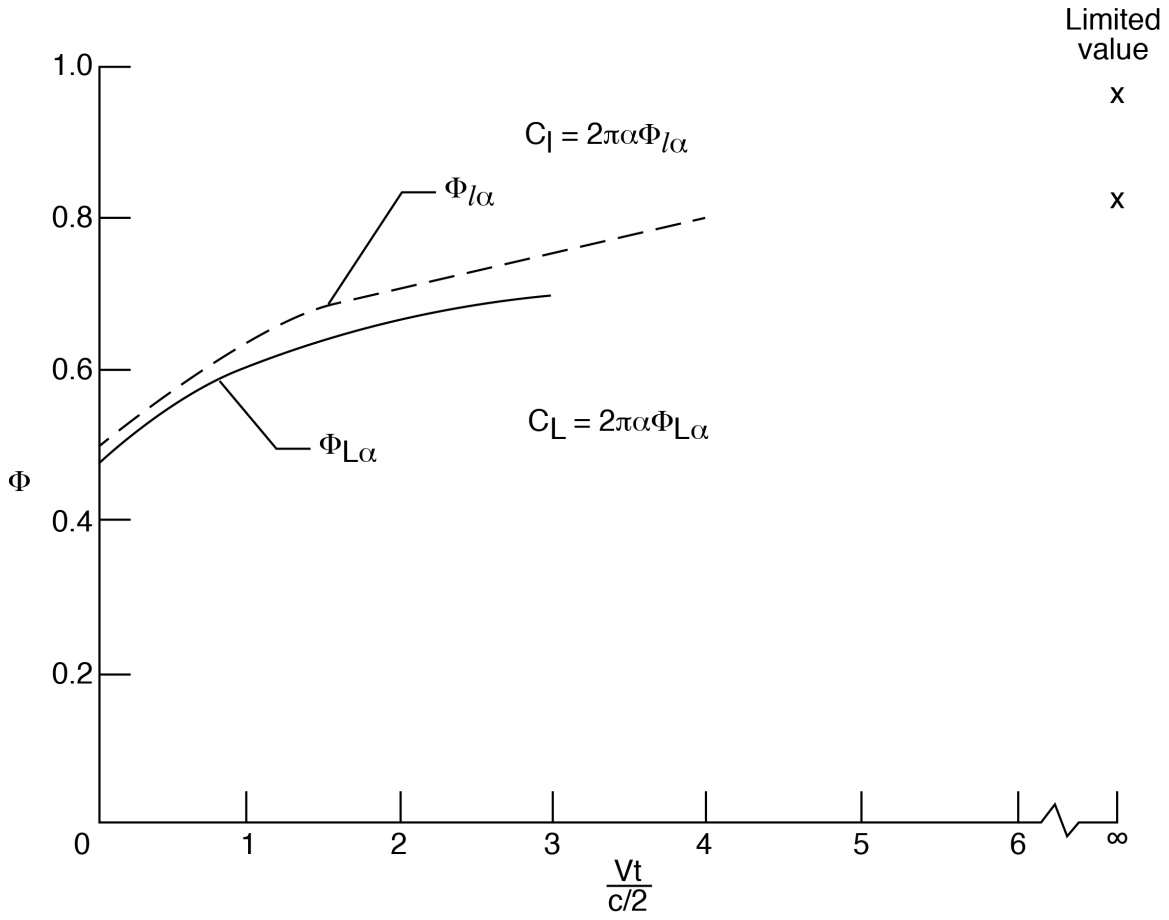

Figure 5. Comparison of lift indicial function due to α for A=4 rectangular wing and two dimensional airfoil (single vortex representation)

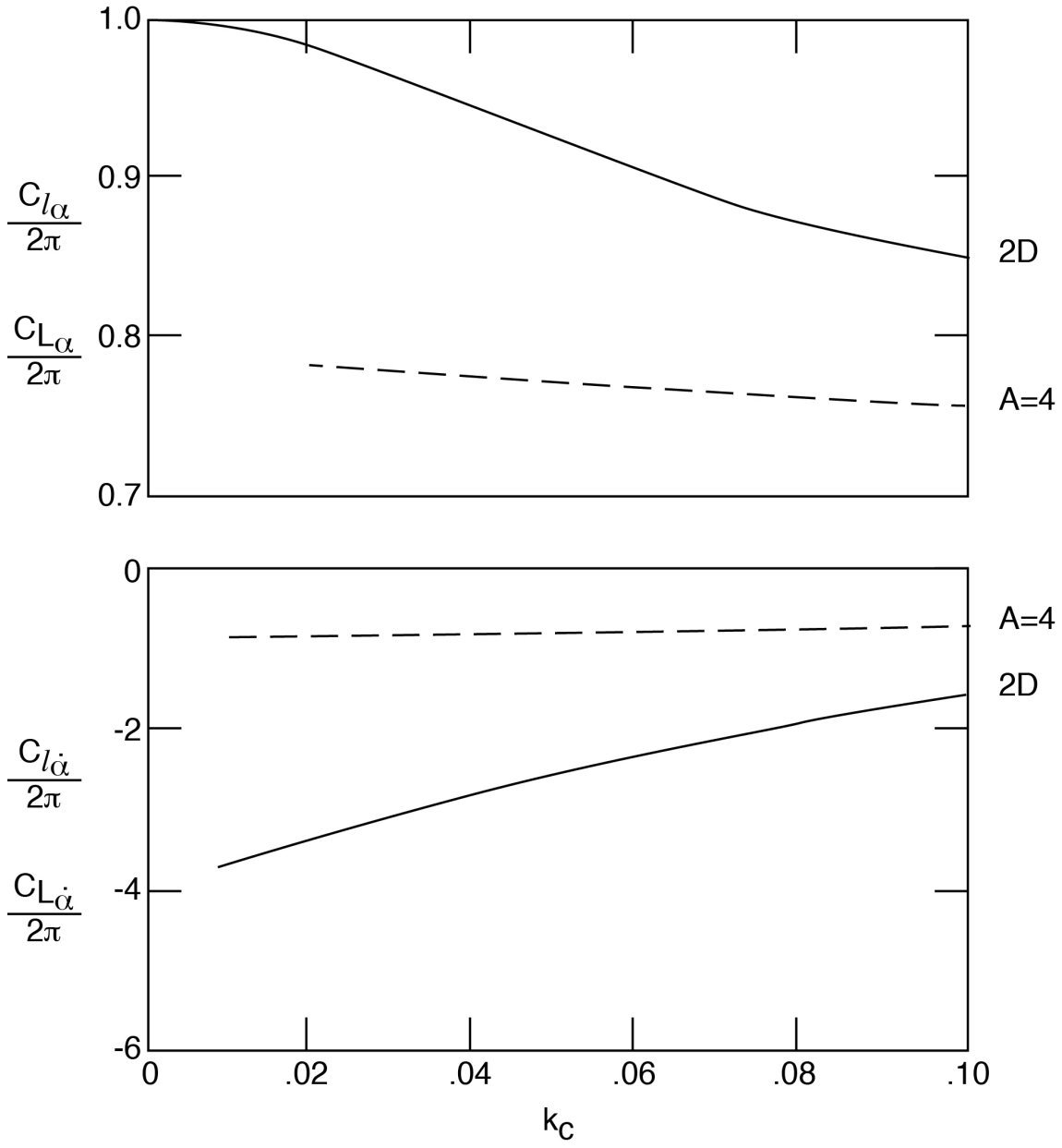

Figure 6. Comparison of unsteady lift aerodynamic derivatives for a two-dimensional airfoil with A=4 rectangular wing using only a single vortex spanwise

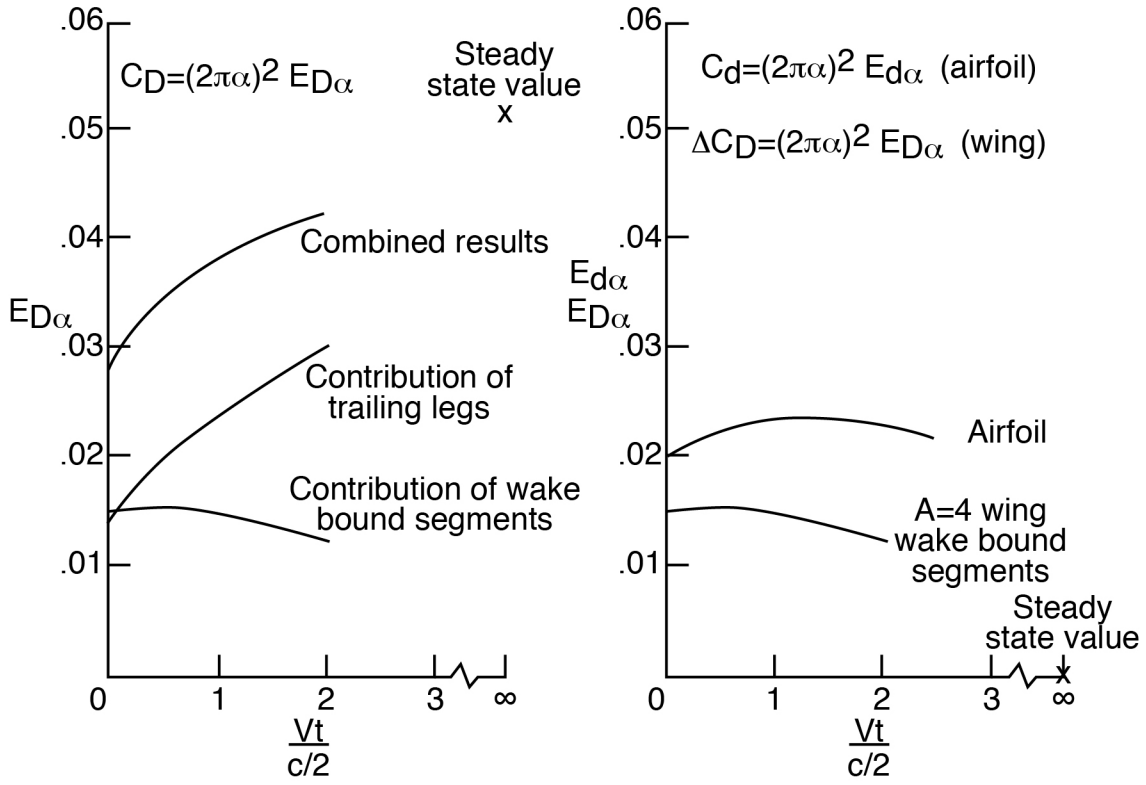

Figure 7. Drag versus $\frac{Vt}{c/2}$ functions due to α (single vortex representation)

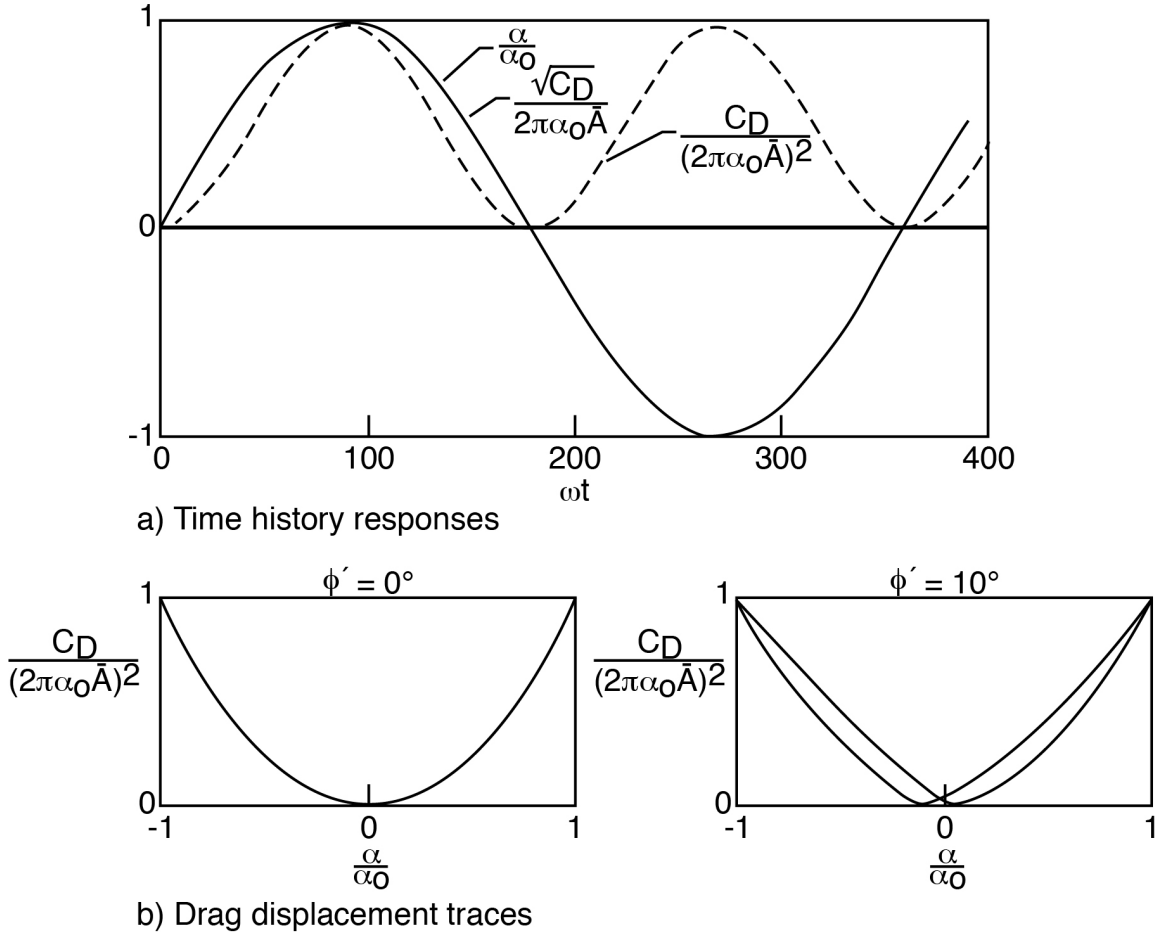

Figure 8. Typical curves of induced drag information due to sinusoidal plunging oscillations in angle of attack

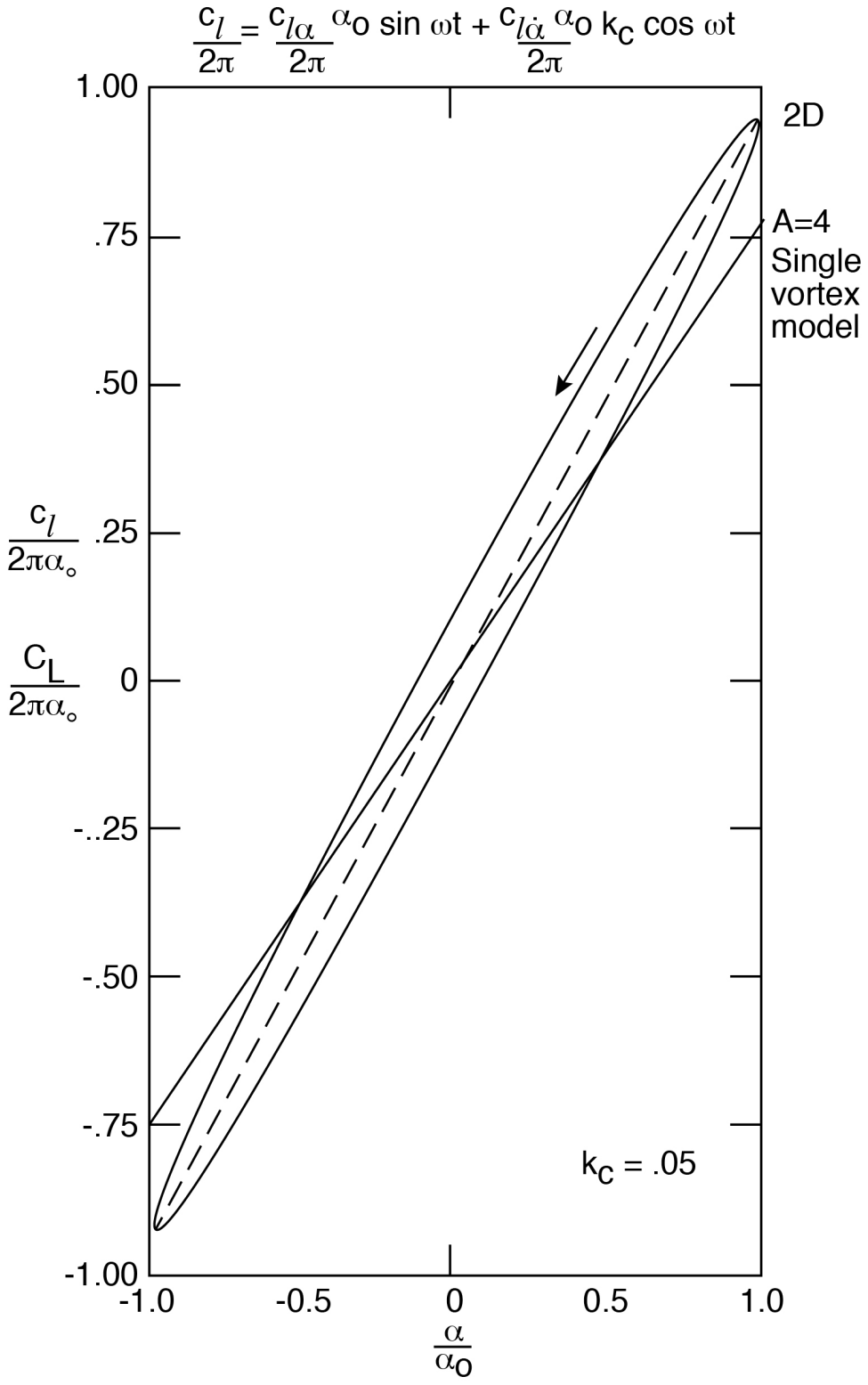

Figure 9. Comparison of lift-displacement traces for a sinusoidal oscillation in angle of attack

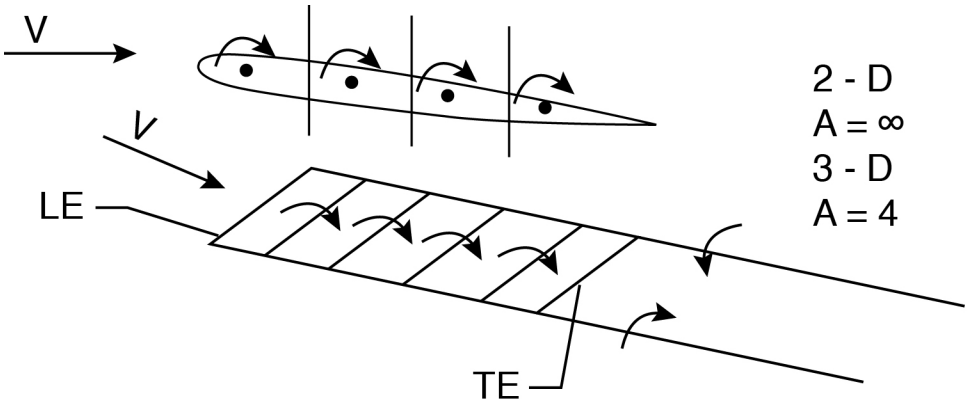

a) Steady state, $\frac{Vt}{c/2} = \infty$

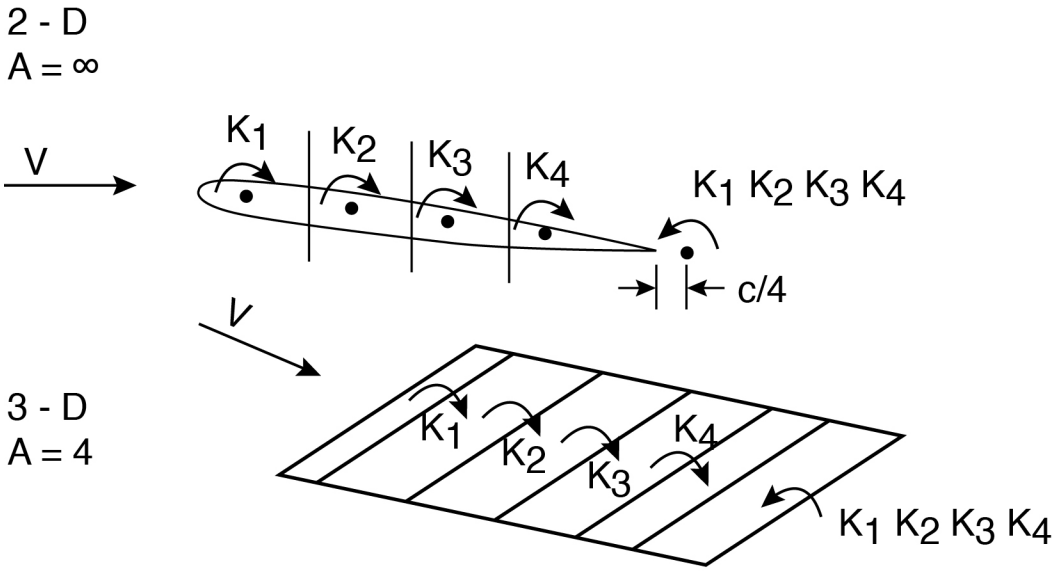

b) Time dependent at t = 0, $\frac{Vt}{c/2} = 0$

Figure 10. Sketches illustrating four computational models

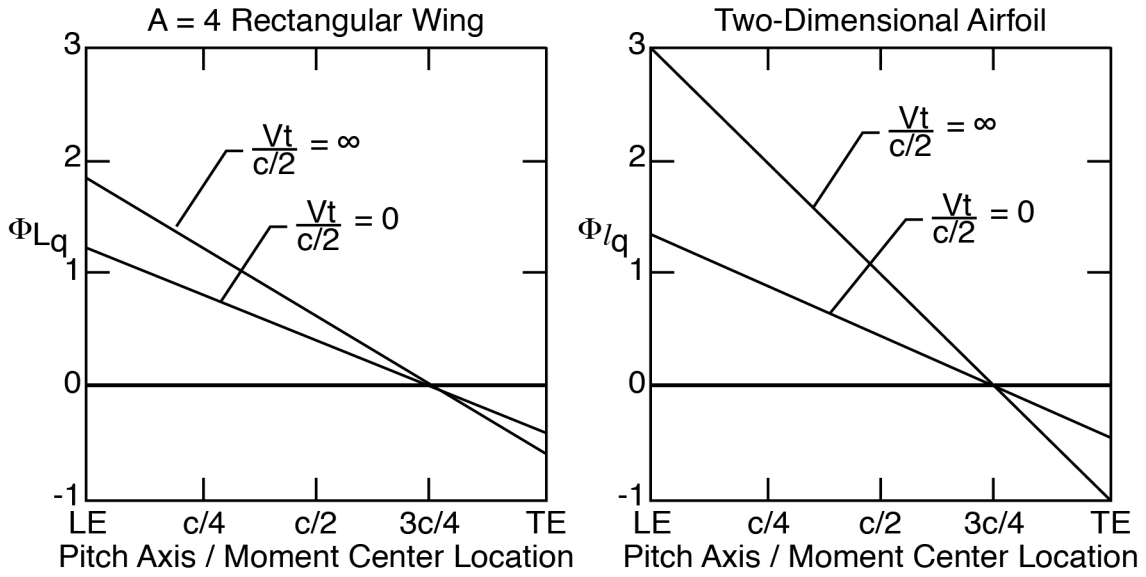

Figure 11. Aspect ratio comparison of chordwise variations of lift indicial functions due to pitch rate

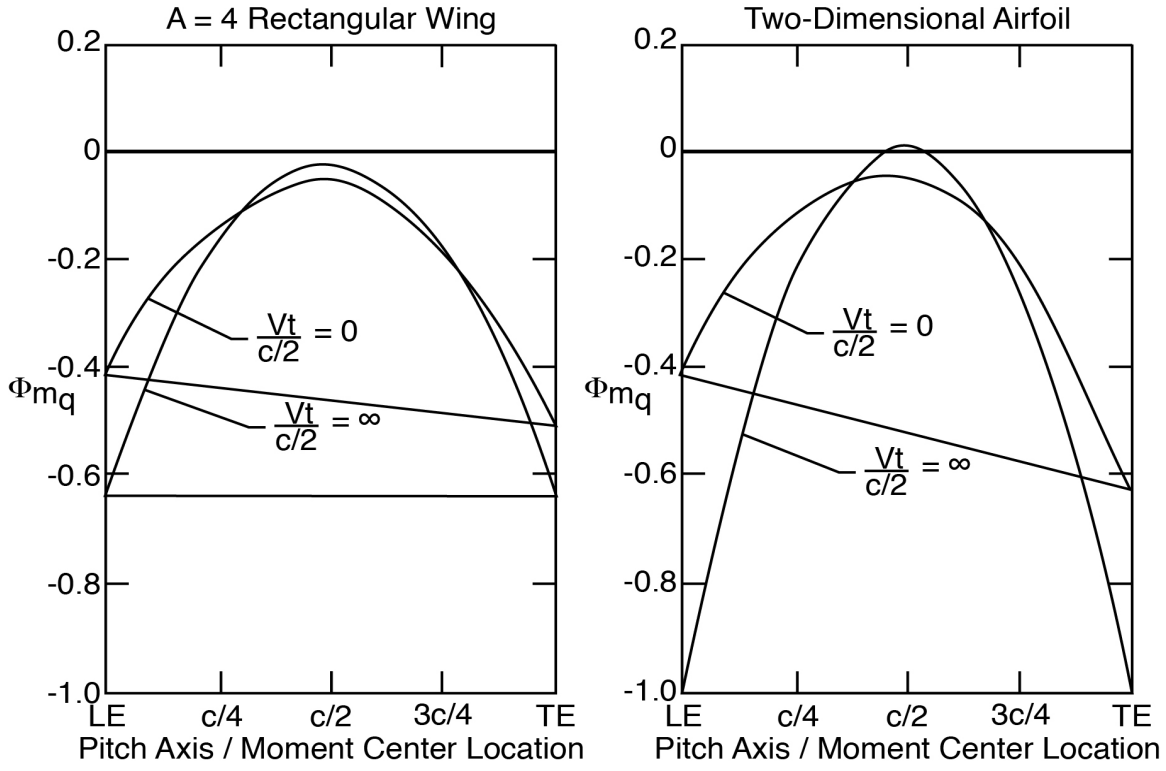

Figure 12. Aspect ratio comparison of chordwise variations of pitching-moment indicial functions due to pitch rate

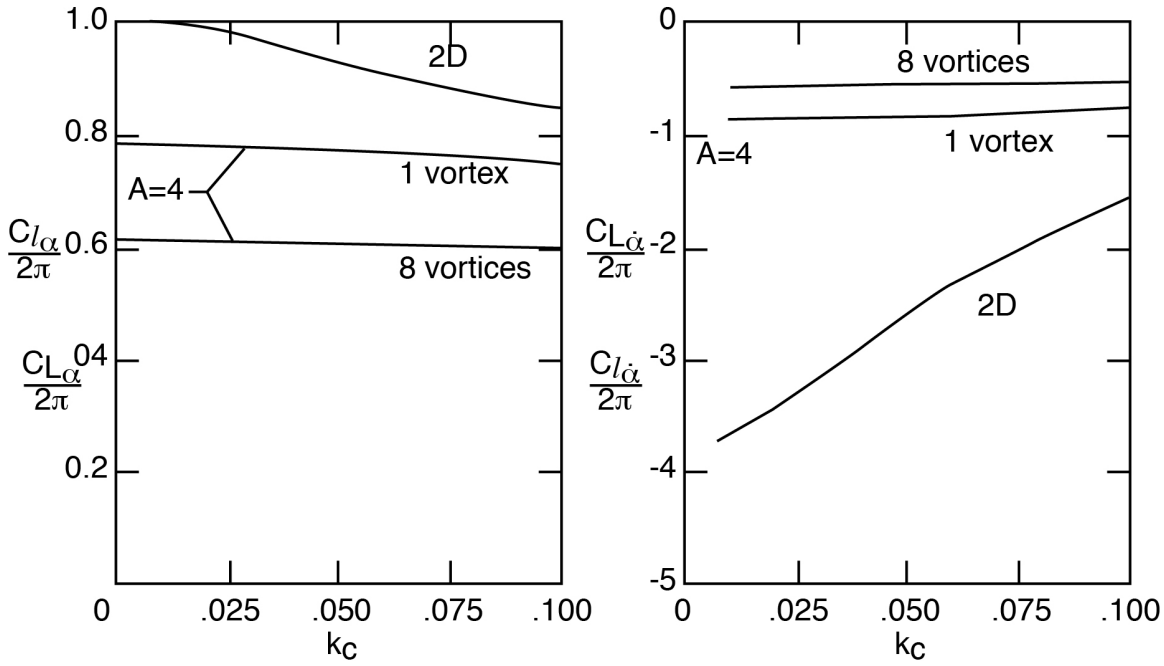

Figure 13. Unsteady lift aerodynamic derivatives for a two dimensional airfoil compared to an A=4 rectangular wing using one or eight vortices spanwise

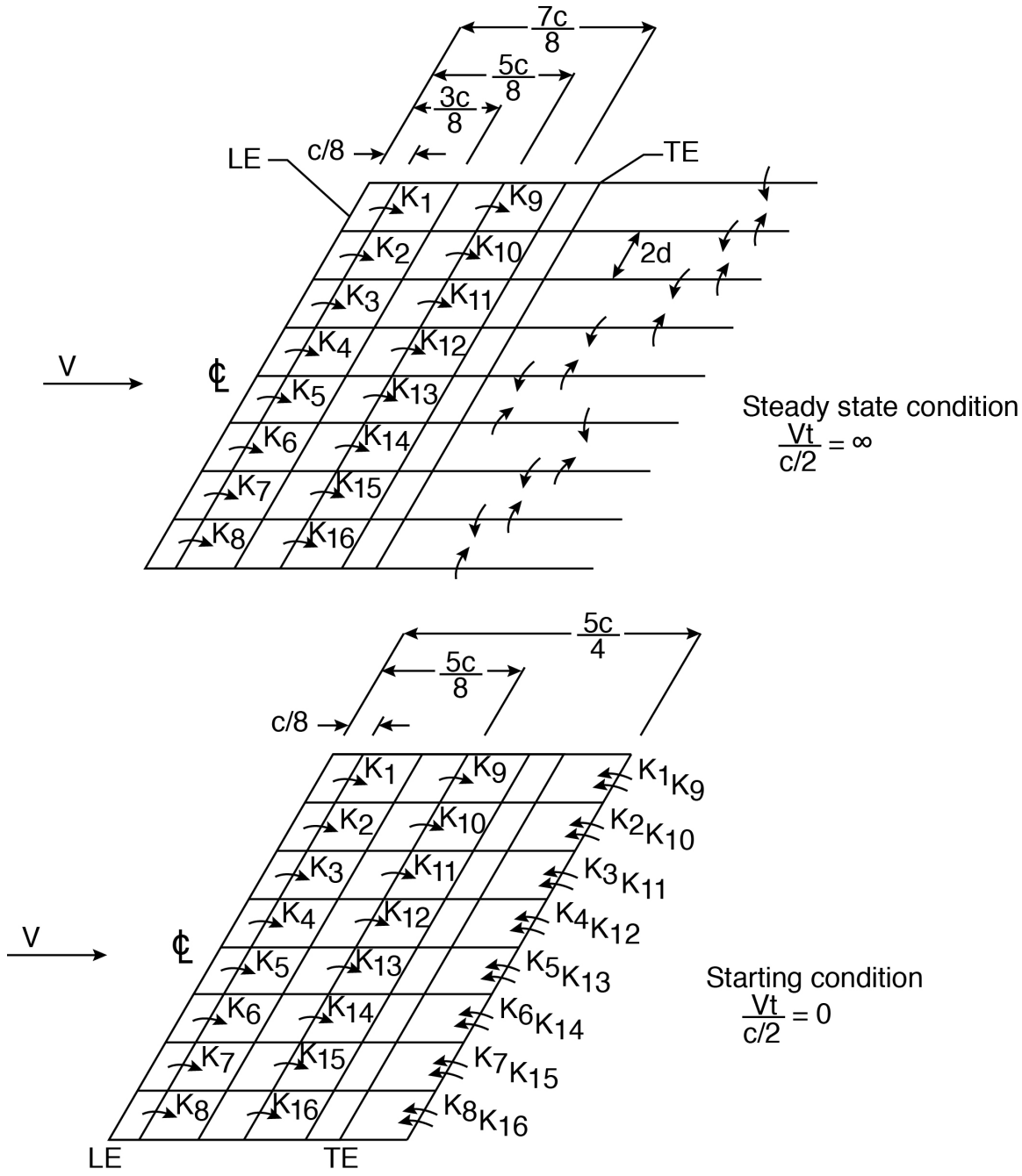

Figure 14. Horseshoe vortex layouts for pitch-rate calculations

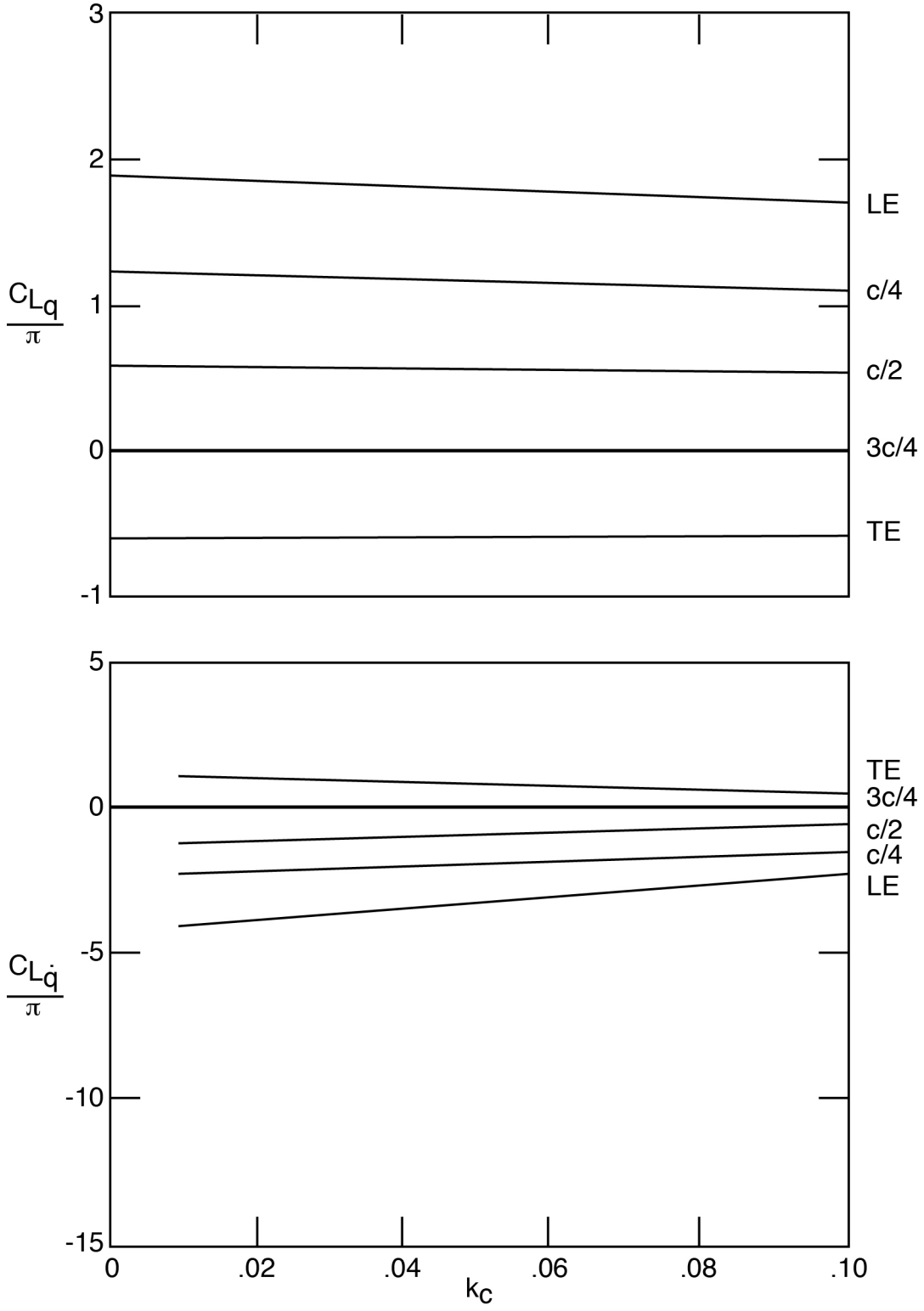

Figure 15. Lift derivatives for sinusoidal oscillations in pitch rate holding α constant at zero

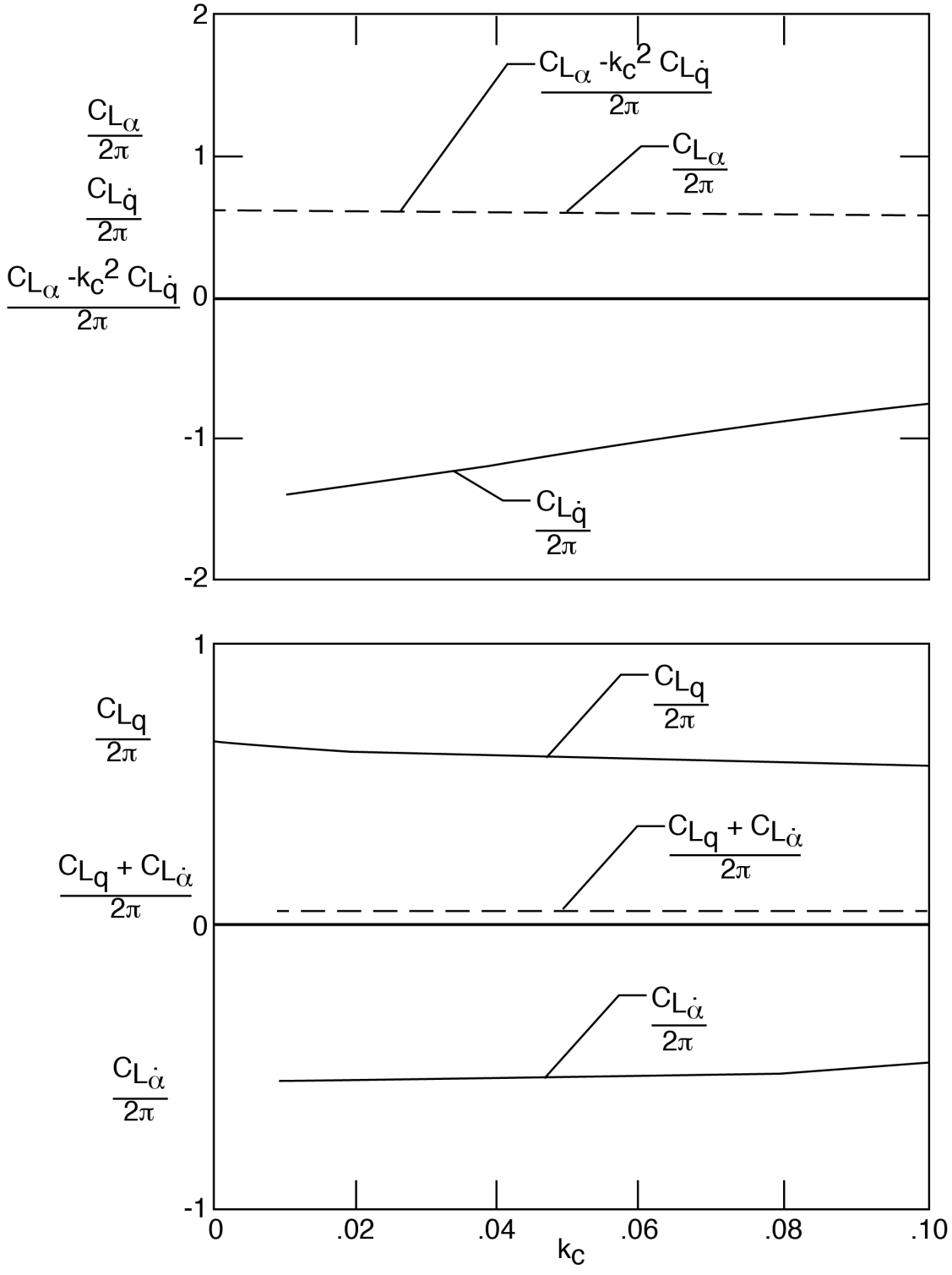

Figure 16. Lift derivatives for A=4 rectangular wing pitching about quarter-chord location showing individual components and combined result

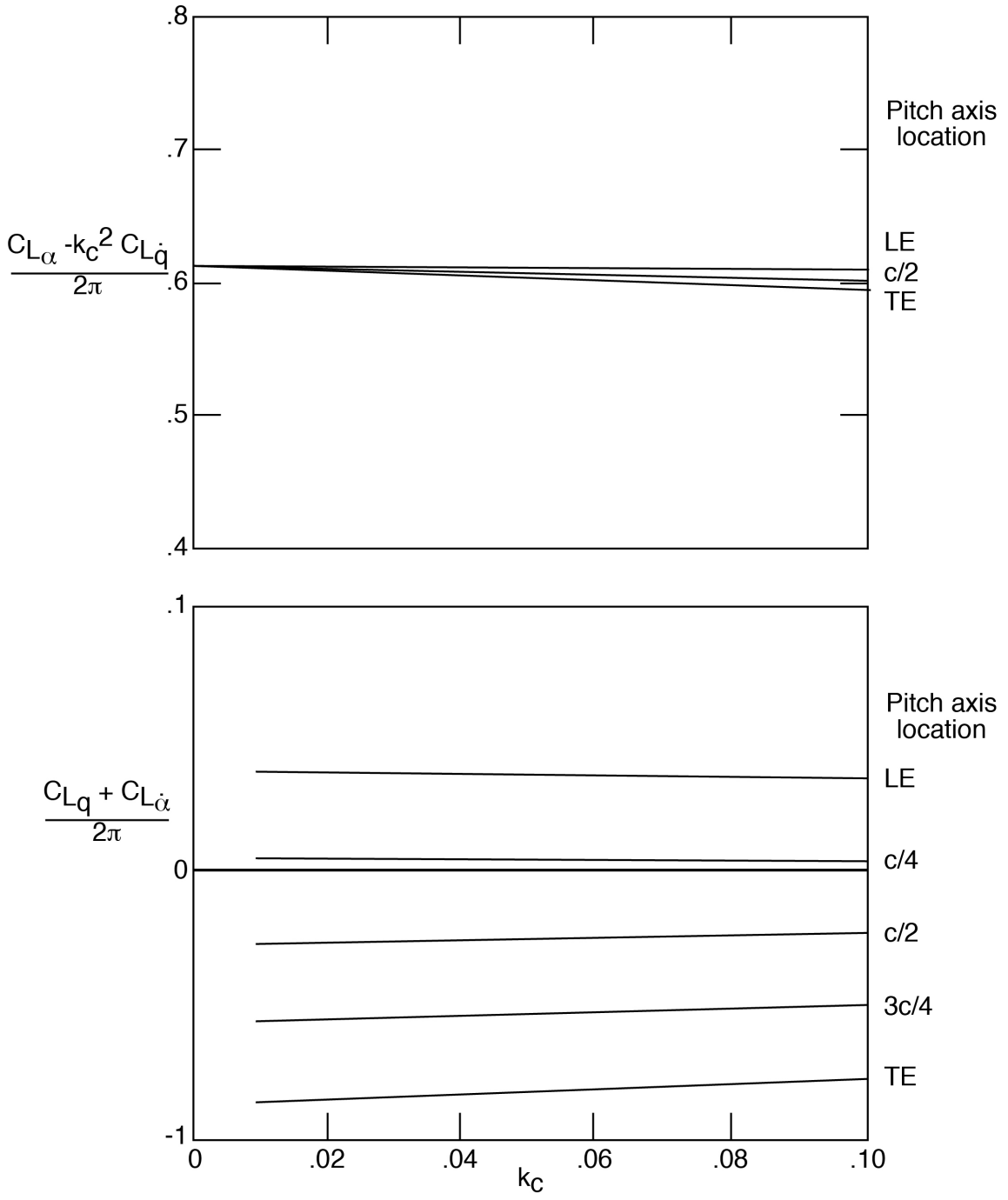

Figure 17. Lift derivatives for an A=4 rectangular wing oscillating sinusoidally about a point on the chord

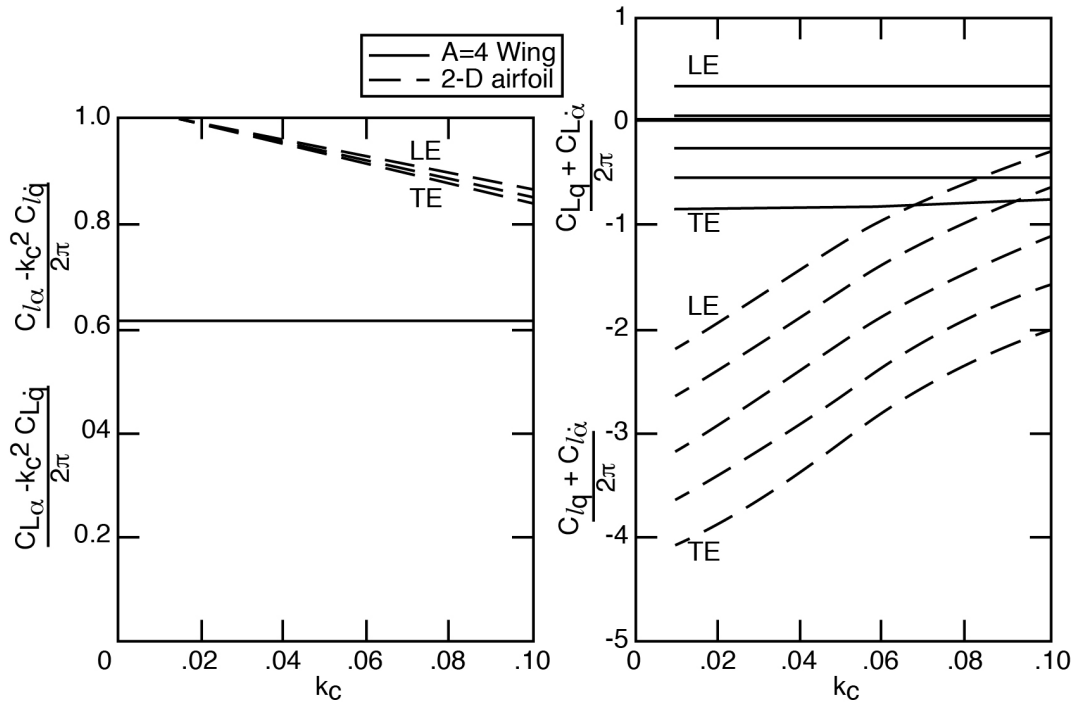

Figure 18. Comparison of oscillating lift derivatives for an A=4 rectangular wing and two-dimensional airfoil for five pitch-axis/moment-center locations

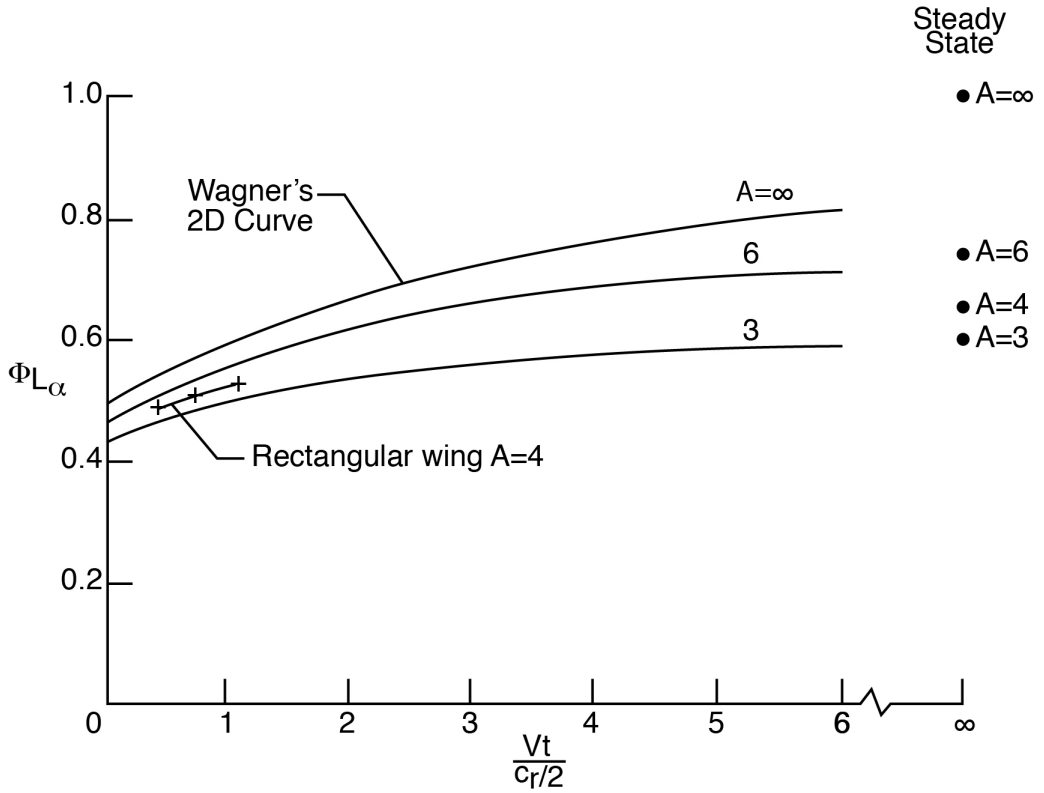

Figure 19. Some lift-indicial function data points for an A=4 rectangular wing due to α using adjusted abscissa values compared with results for A=3 and A=6 elliptical wings, where the abscissa is distance traveled in root semi-chords of the elliptical planform

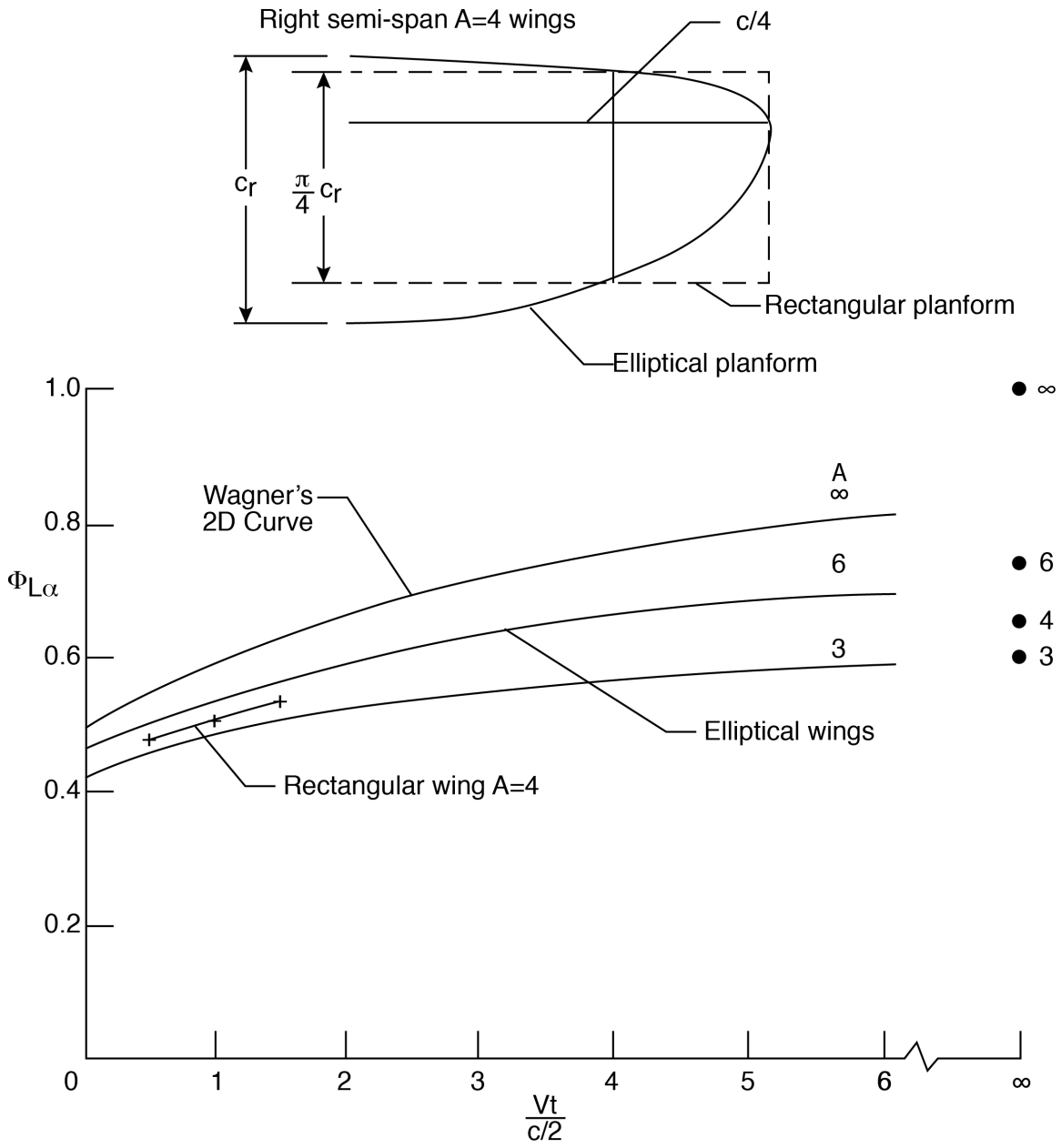

Figure 20. Comparison of lift-indicial functions due to α for rectangular and elliptical wings versus distance traveled in half-chords of the rectangular wing

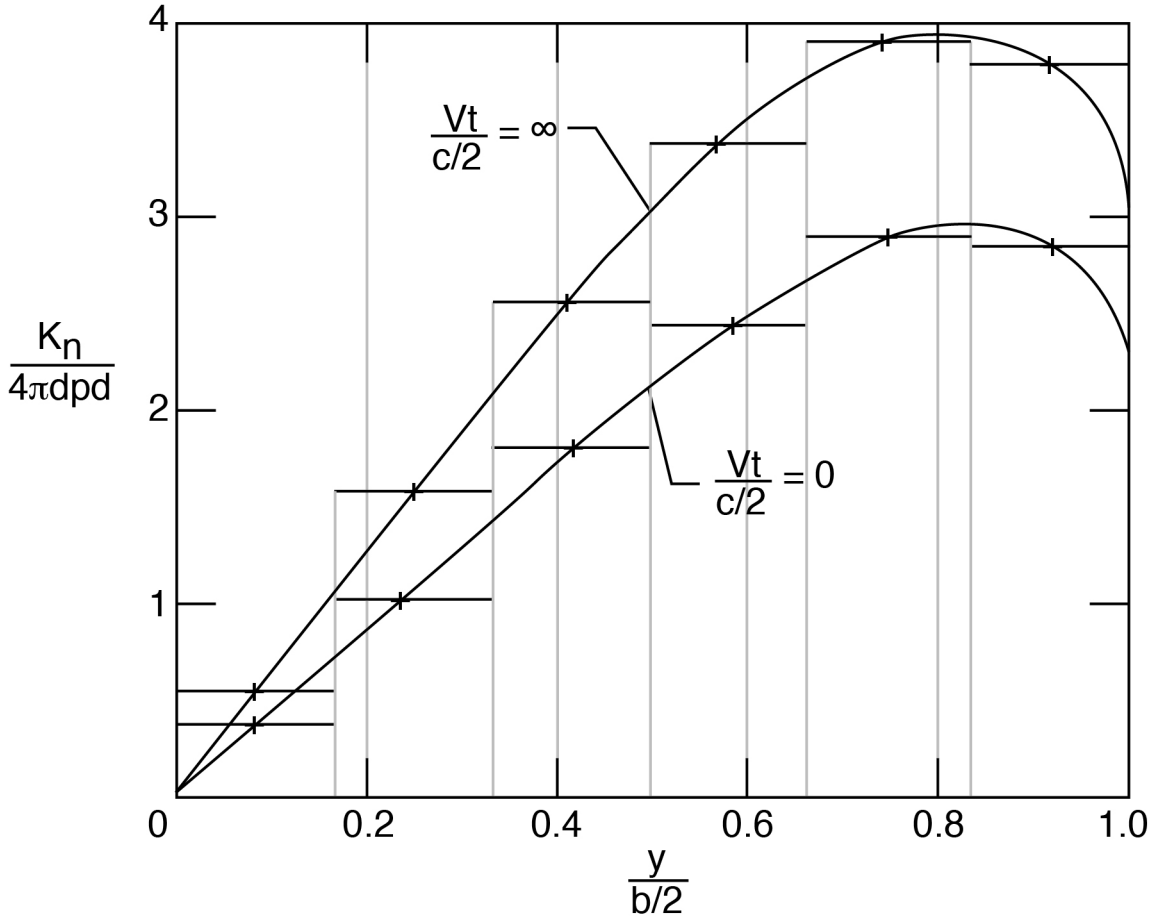

Figure 21. Right wing semi-span load distributions due to roll rate using 12 vortices spanwise

$$C_{l_p} = -.575746\ \Phi_{\ell p}$$

$$\Phi_{\ell p} = 1 - .09497e^{\left(-\frac{3}{8}\ \frac{Vt}{c/2}\right)} - .18794e^{\left(-\frac{7}{8}\ \frac{Vt}{c/2}\right)}$$

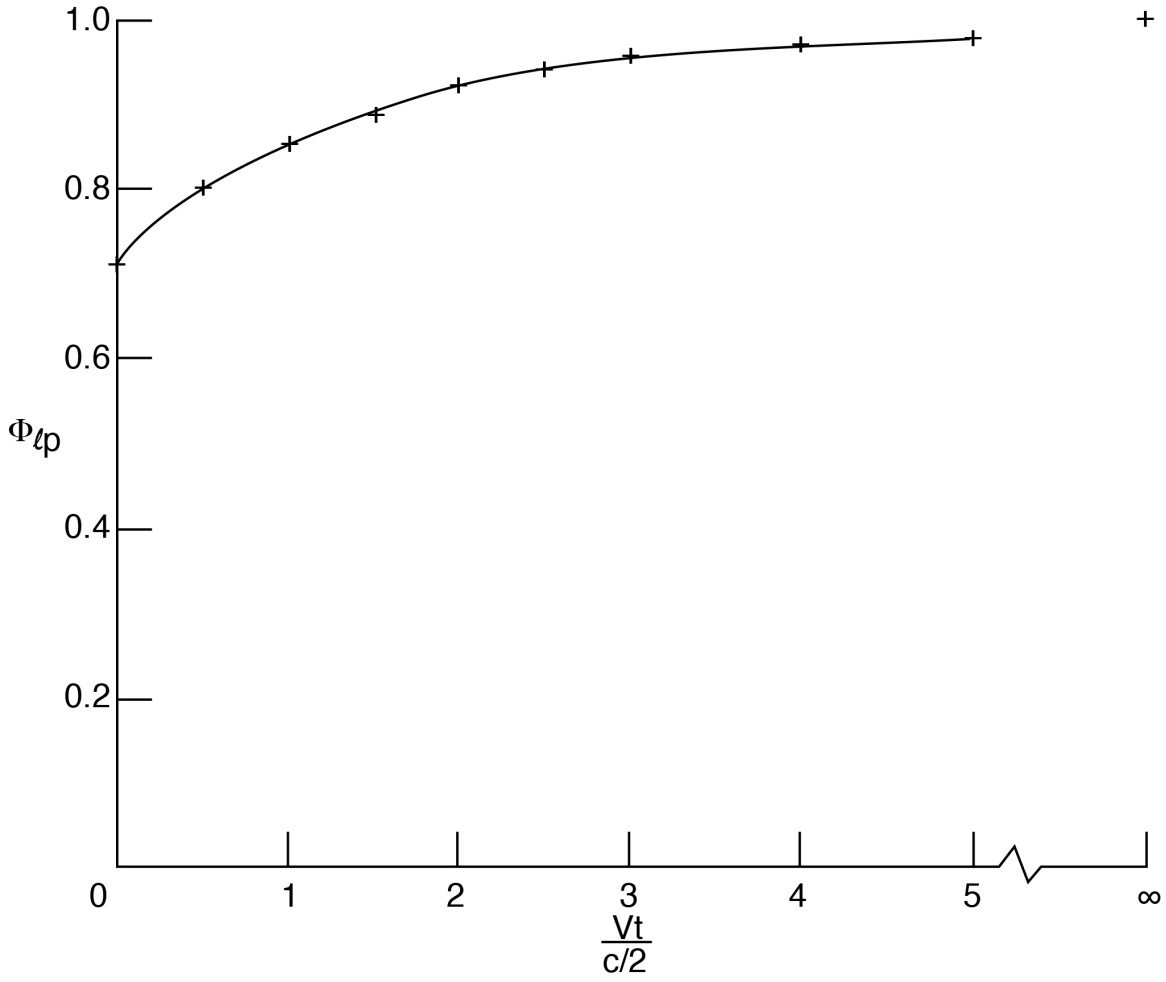

Figure 22. Indicial function for roll rate for an A=8 rectangular wing

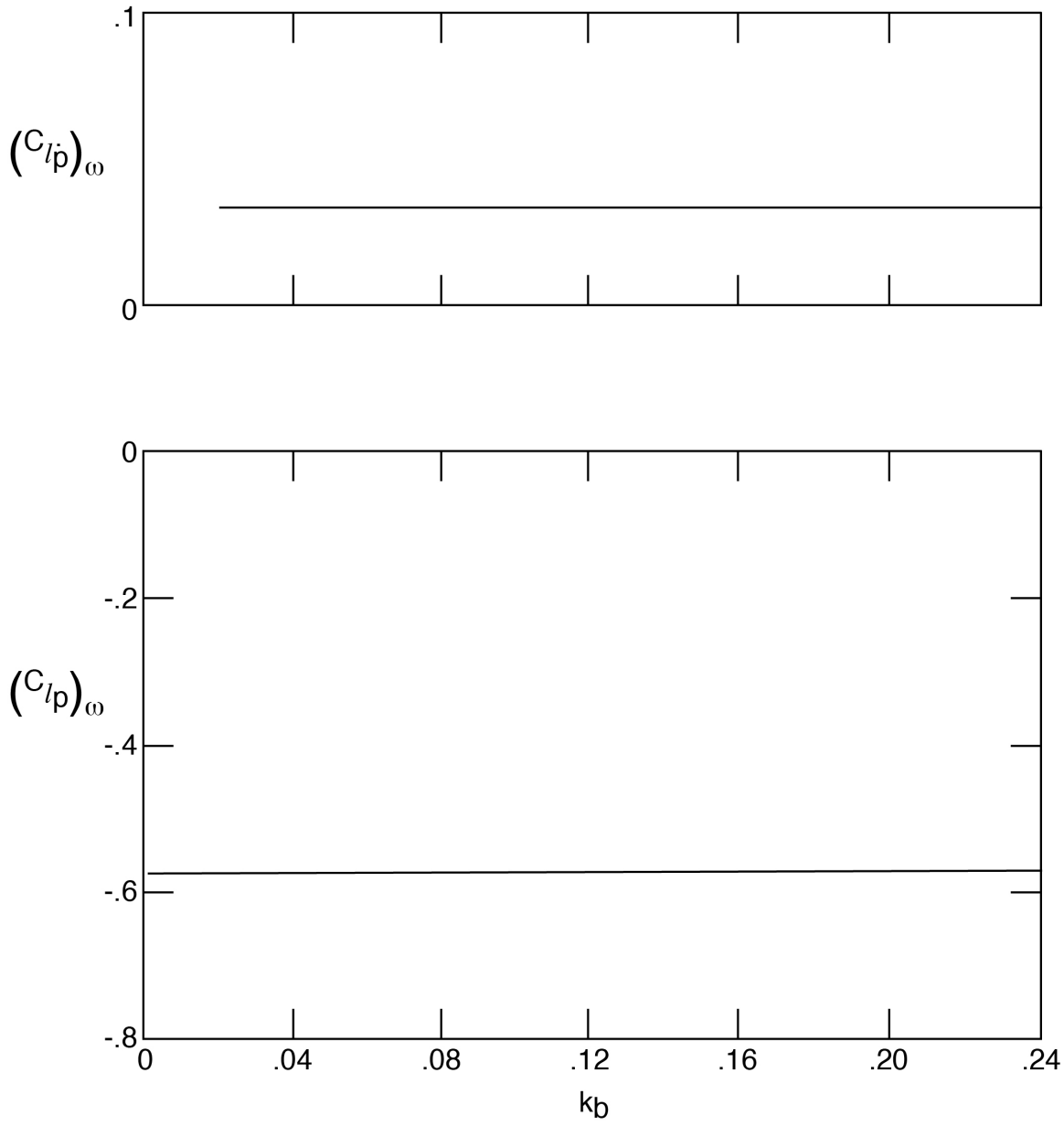

Figure 23. Rolling moment derivatives for sinusoidal oscillations in roll about the velocity vector for an A=8 rectangular wing

$$C_l = C_{lp}\frac{pb}{2v} + C_{l\dot{p}}\dot{p}\left(\frac{b}{2V}\right)^2$$

$$\phi = \phi_o \sin \omega t$$

$$p = \dot{\phi} = \phi_o \omega \cos \omega t$$

$$\dot{p} = \ddot{\phi} = -\phi_o \omega^2 \sin \omega t$$

$$\frac{C_l}{\phi_o} = C_{lp}\, k_b \cos \omega t + C_{l\dot{p}}(-k_b^2 \sin \omega t)$$

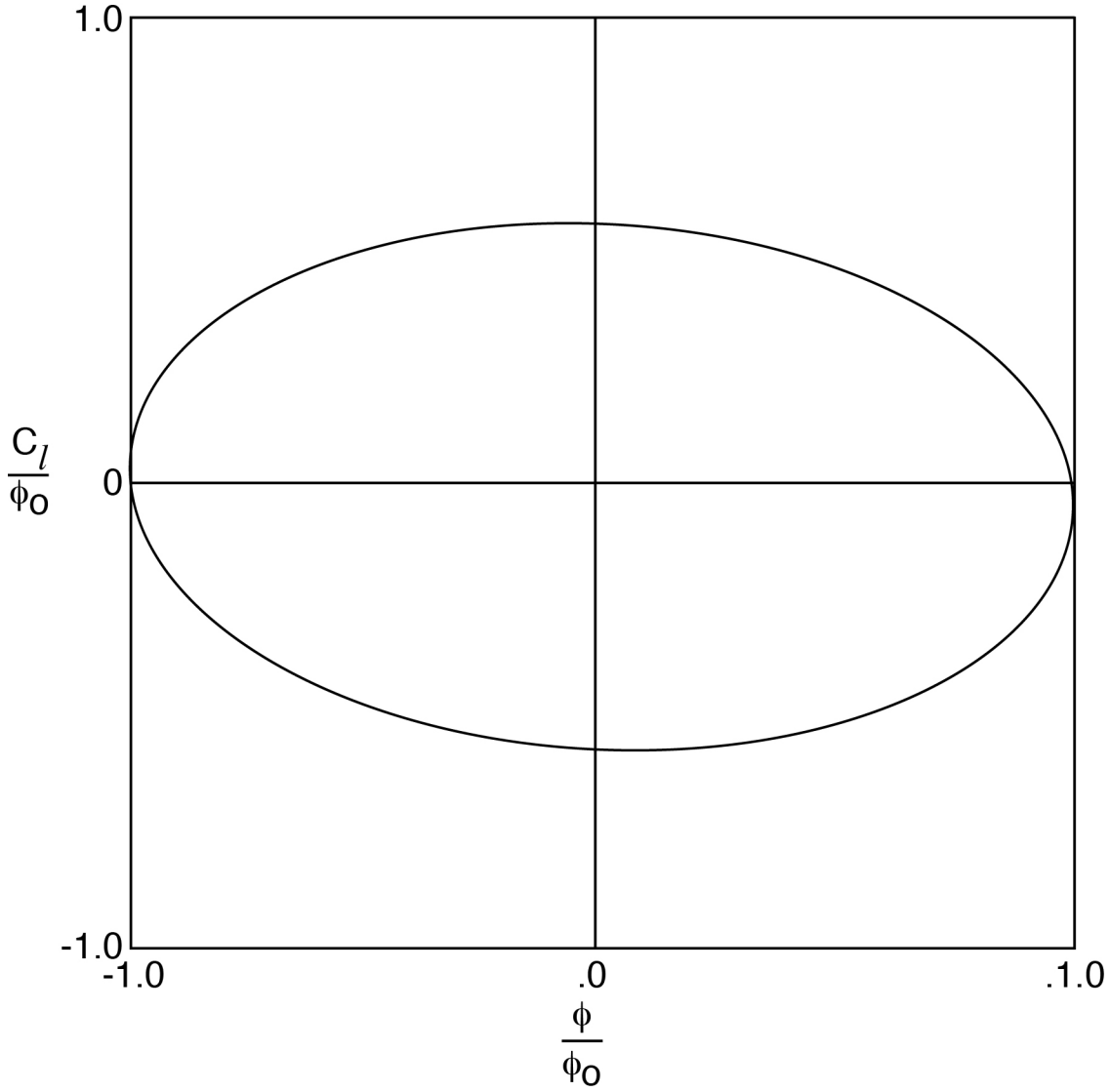

Figure 24. Example of rolling moment displacement trace for an A=8 rectangular wing

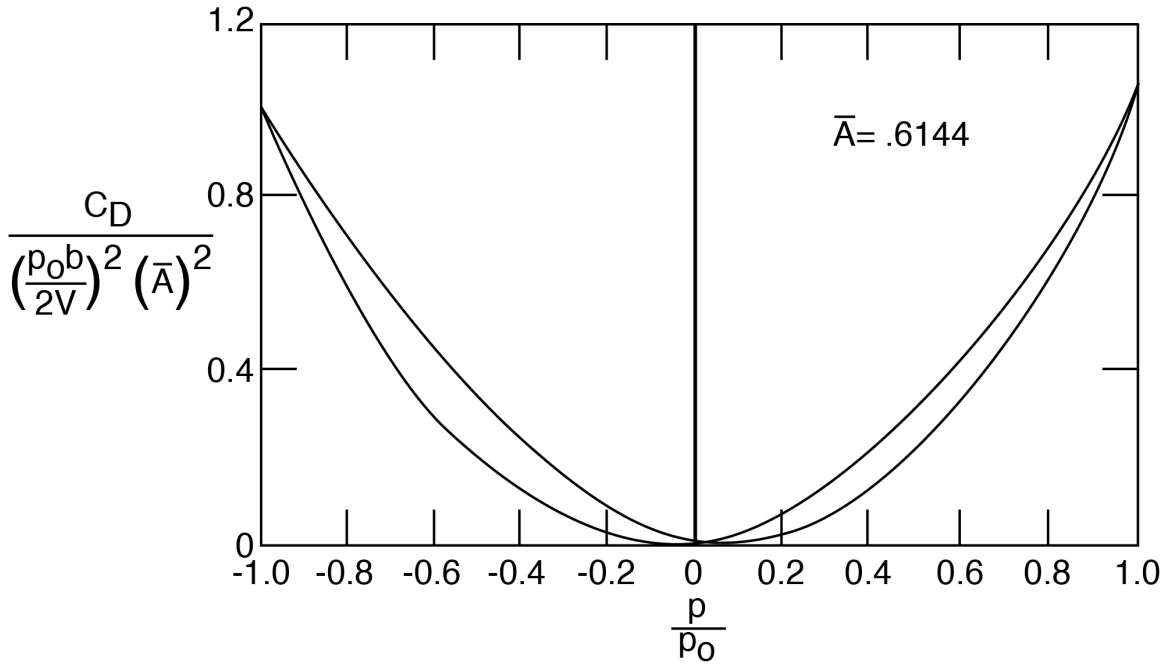

Figure 25. Trace of drag parameter values versus roll-rate ratio for an A=8 rectangular wing

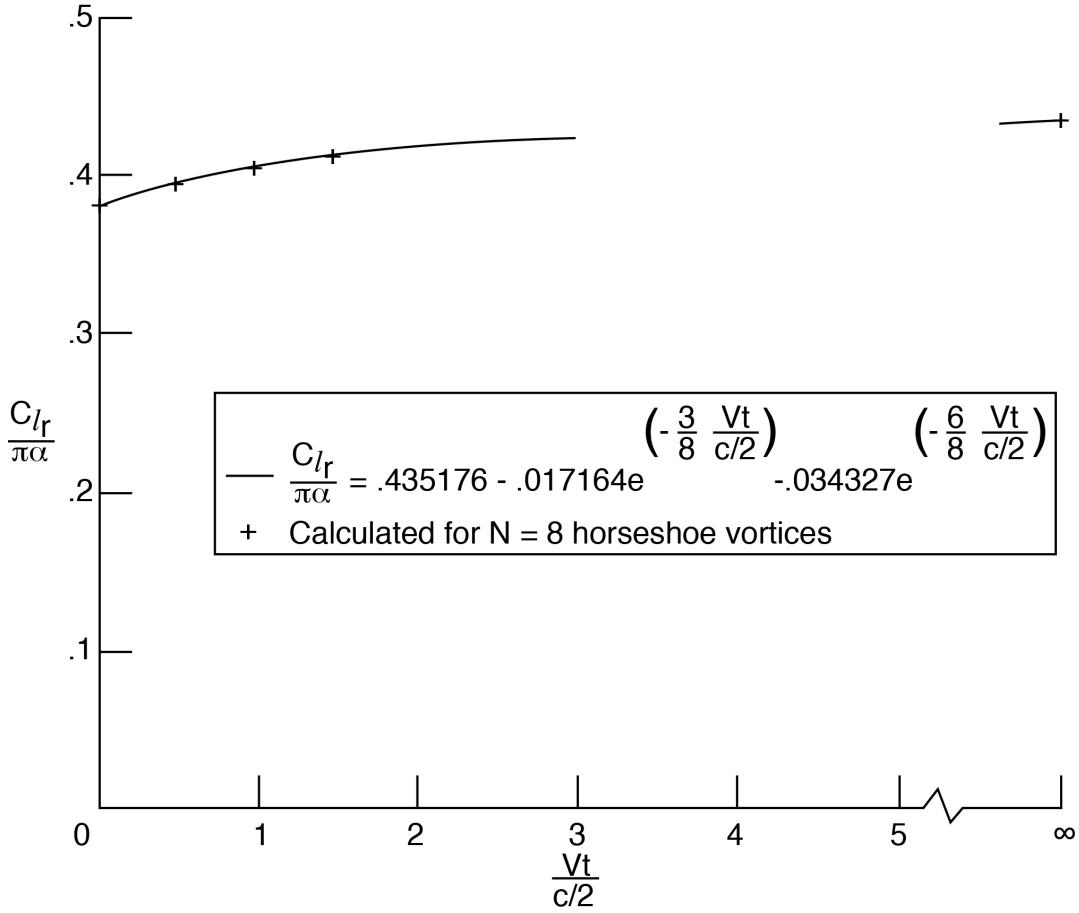

Figure 26. Response due to a step input in yaw rate for an A=8 rectangular wing

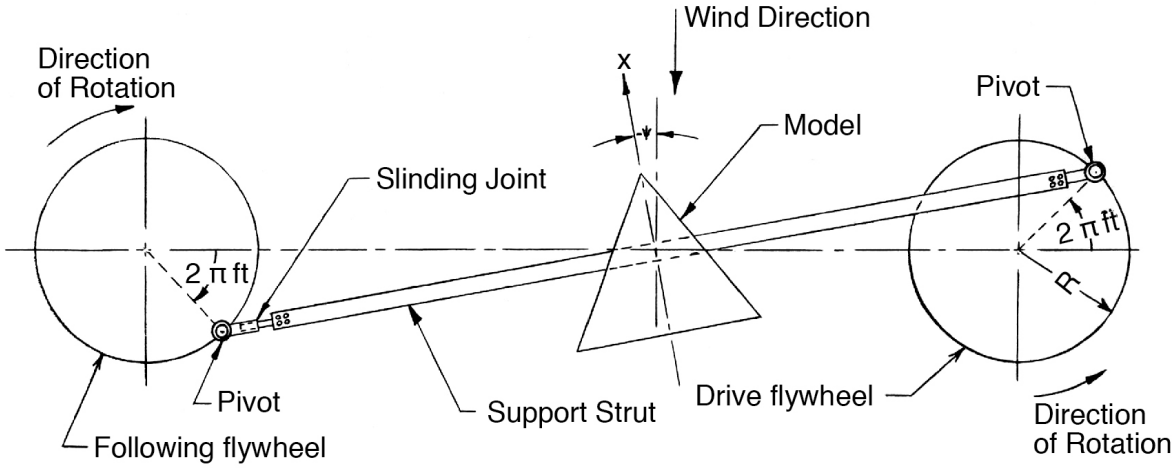

Figure 27. Schematic of mechanism for simulating pure yawing oscillation

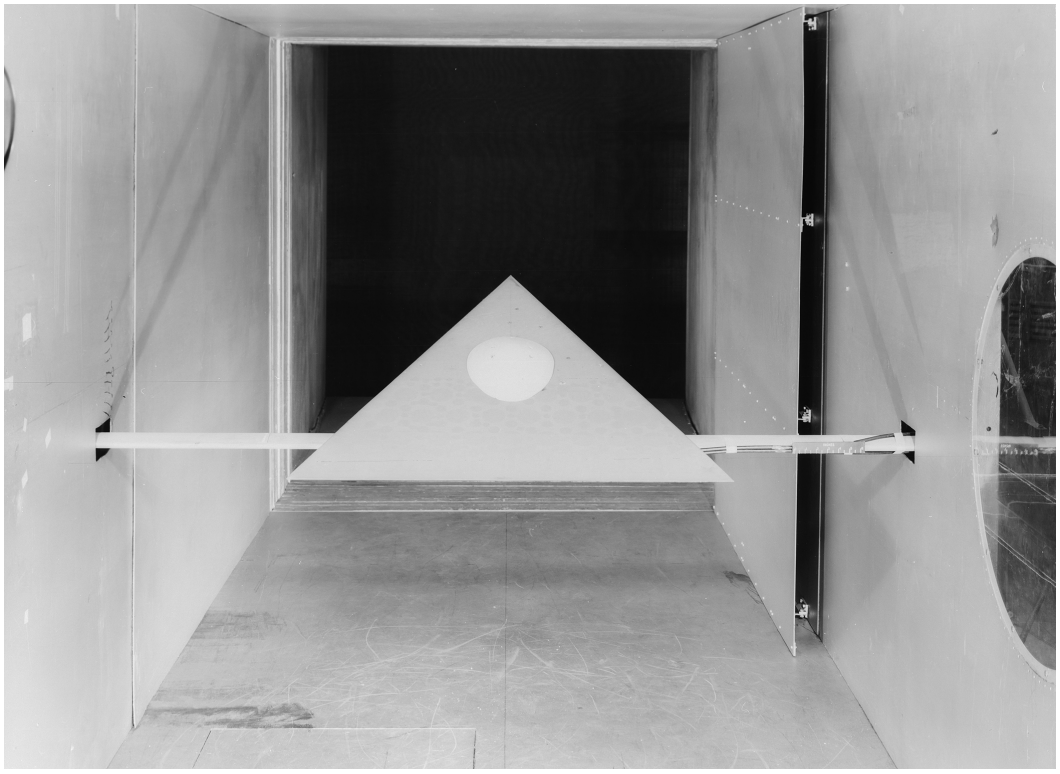

Figure 28a. Sixty-degree delta wing model mounted on the pure-yaw oscillation test rig in the 6- by 6-foot test section of the Langley Stability Tunnel

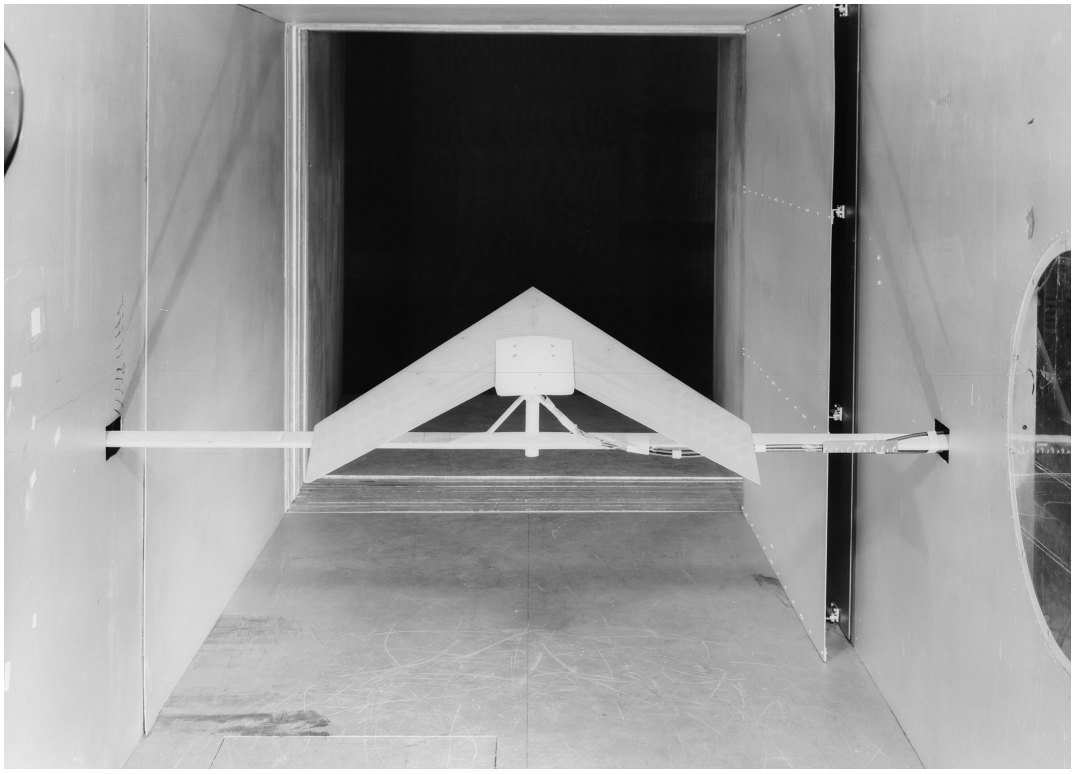

Figure 28b. Forty-five degree swept wing model mounted on the pure-yaw oscillation test rig in the 6- by 6-foot test section of the Langley Stability Tunnel

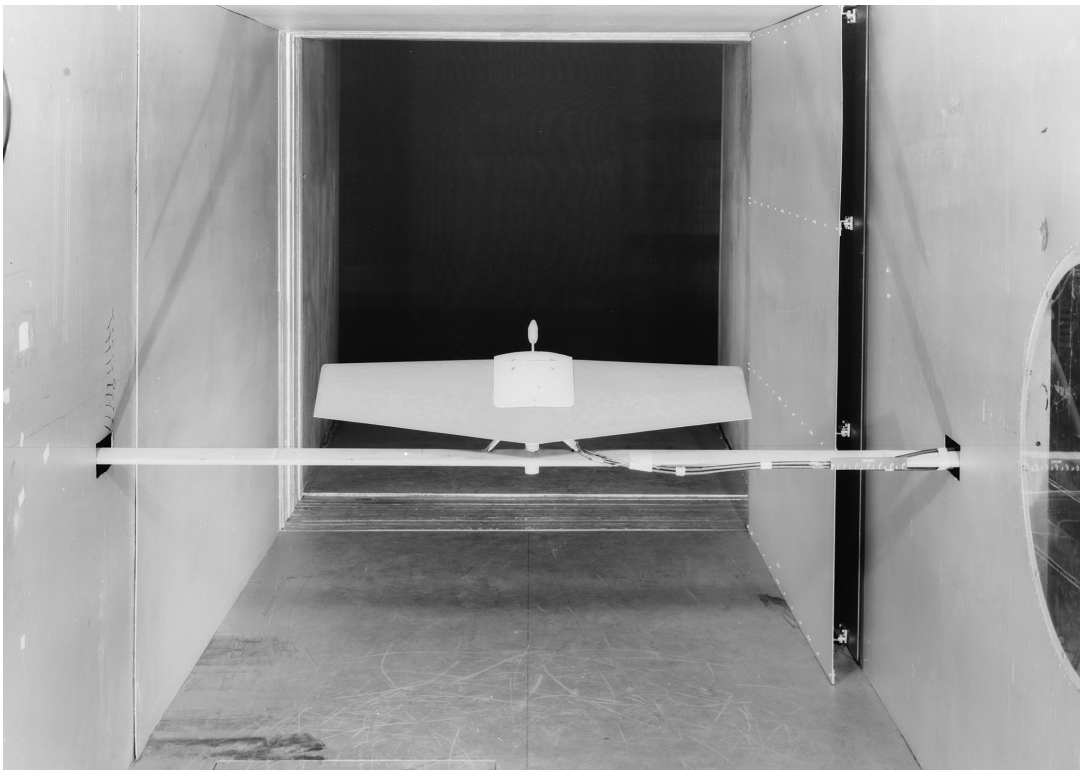

Figure 28c. Unswept wing model mounted on the pure-yaw oscillation test rig in the 6- by 6-foot test section of the Langley Stability Tunnel

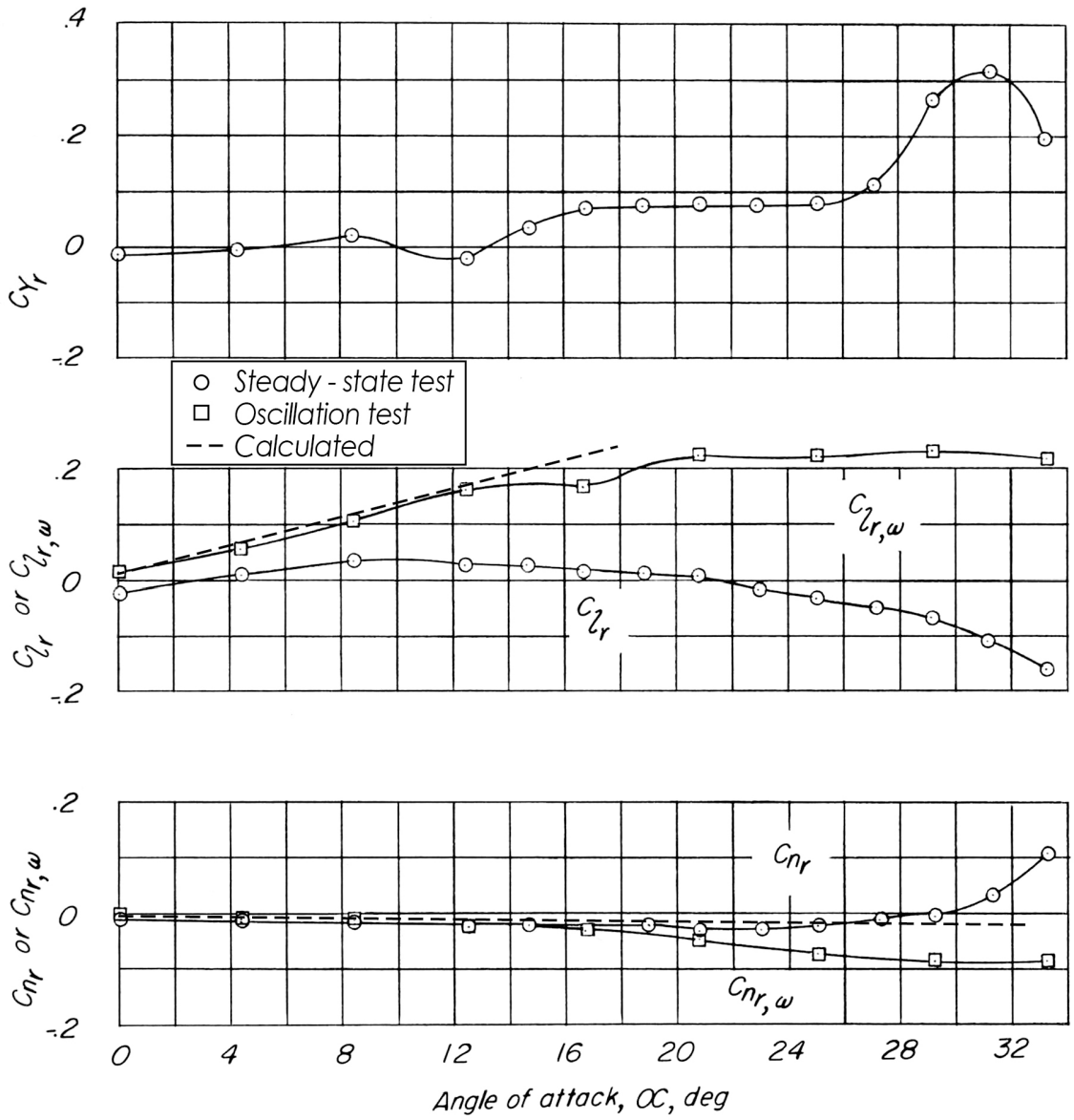

Figure 29a. Derivative values due to yawing velocity from steady-state tests, oscillation tests, and oscillation theory for a 60-degree delta wing

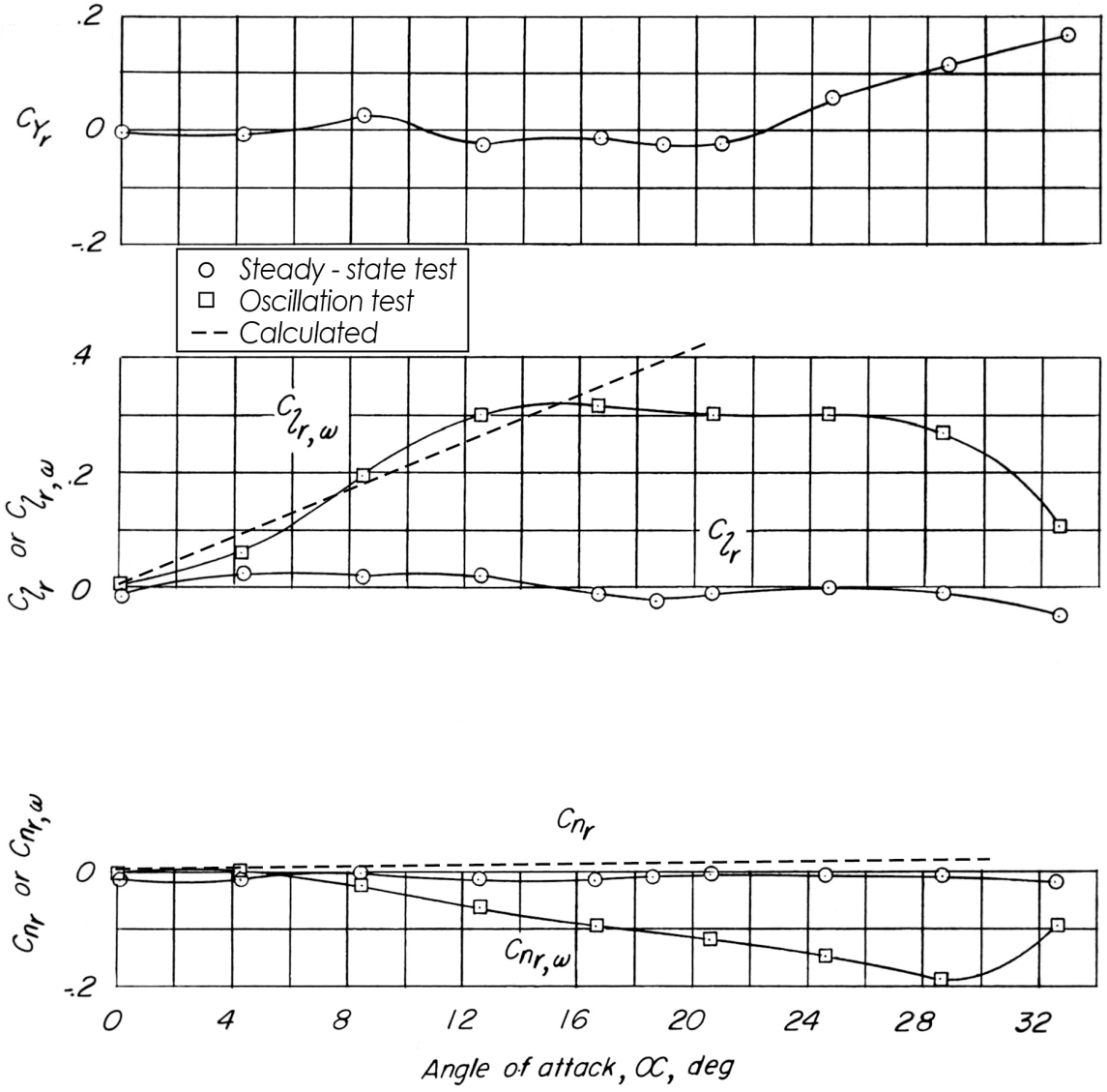

Figure 29b. Derivative values due to yawing velocity from steady-state tests, oscillation tests, and oscillation theory for a 45-degree swept wing

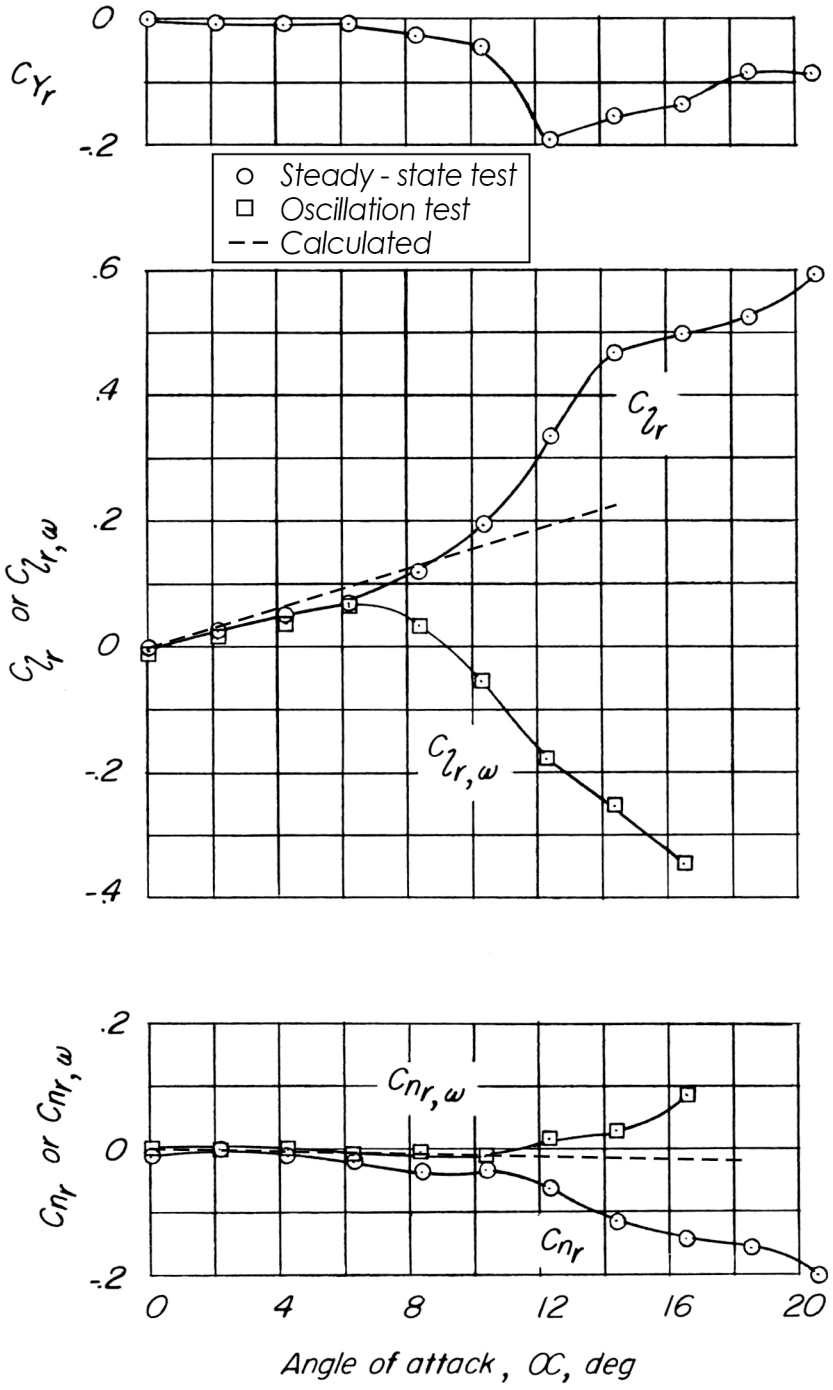

Figure 29c. Derivative values due to yawing velocity from steady-state tests, oscillation tests, and oscillation theory for an unswept wing

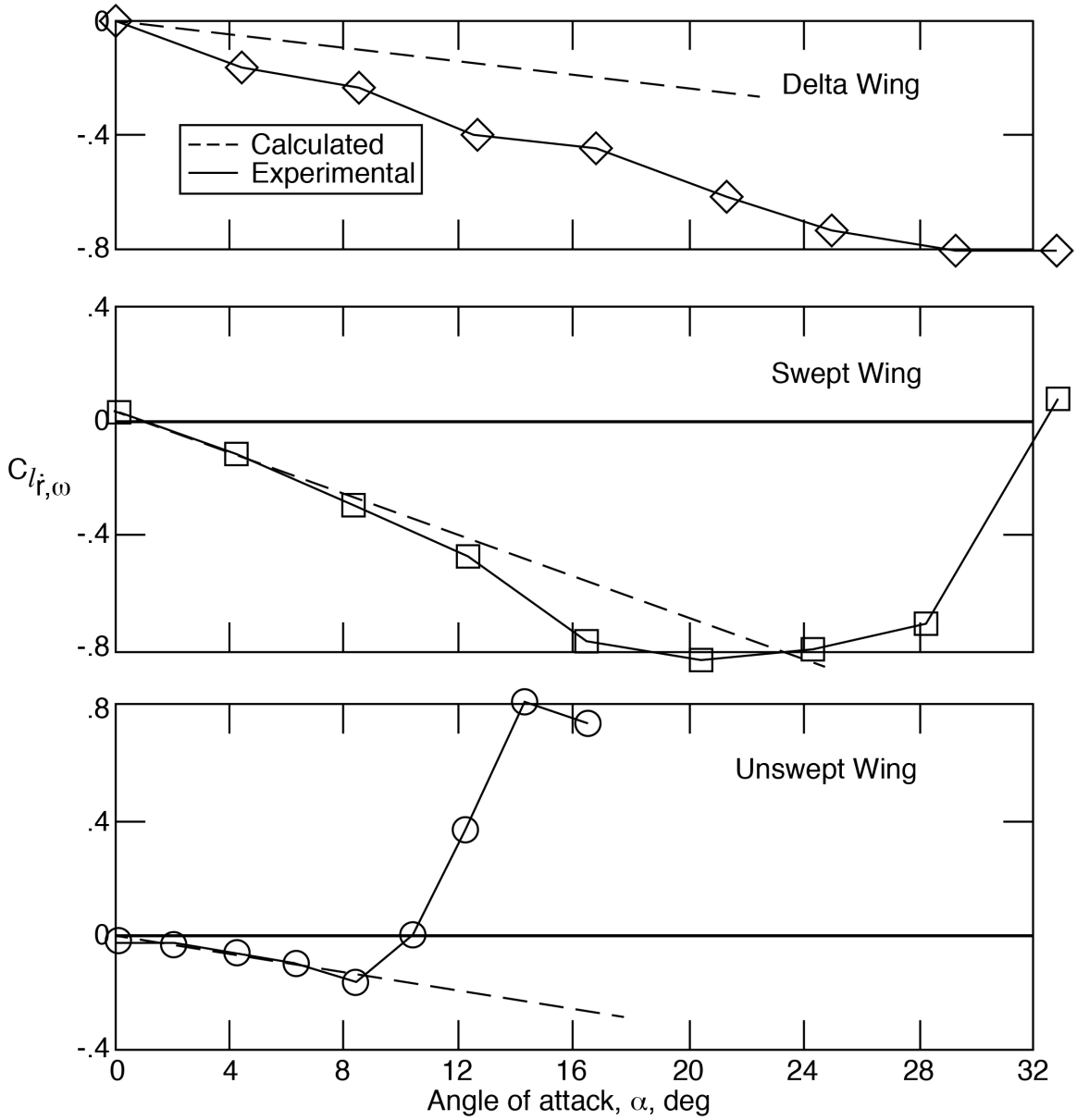

Figure 30. Comparison of calculated and experimental values for rolling moment derivatives due to yawing acceleration $C_{l_{\dot{r},\omega}}$ for three wings (k_b = 0.22)

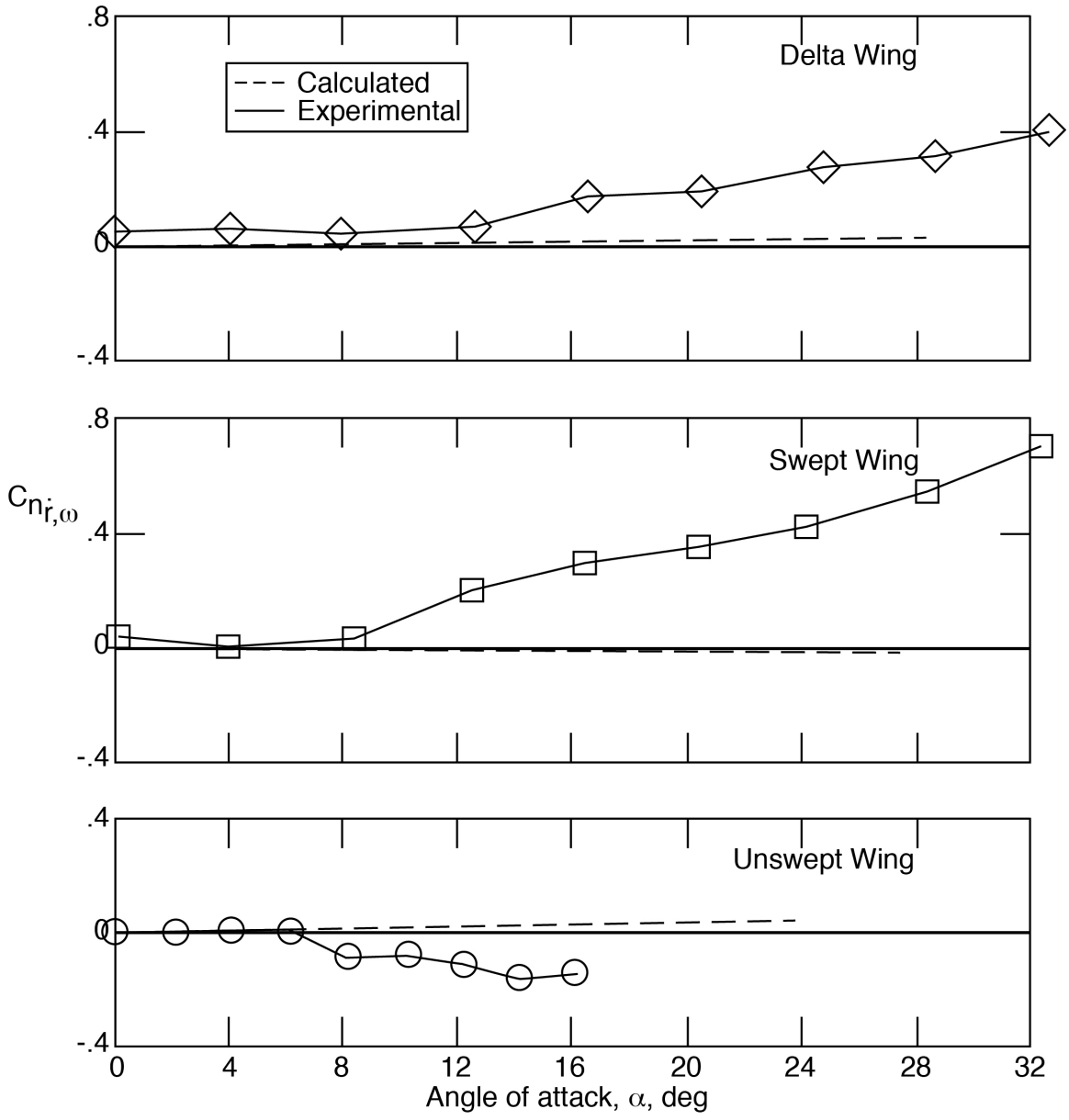

Figure 31. Comparison of calculated and experimental values for yawing moment derivatives due to yawing acceleration $C_{n_{\dot{r},\omega}}$ for three wings (k_b = 0.22)

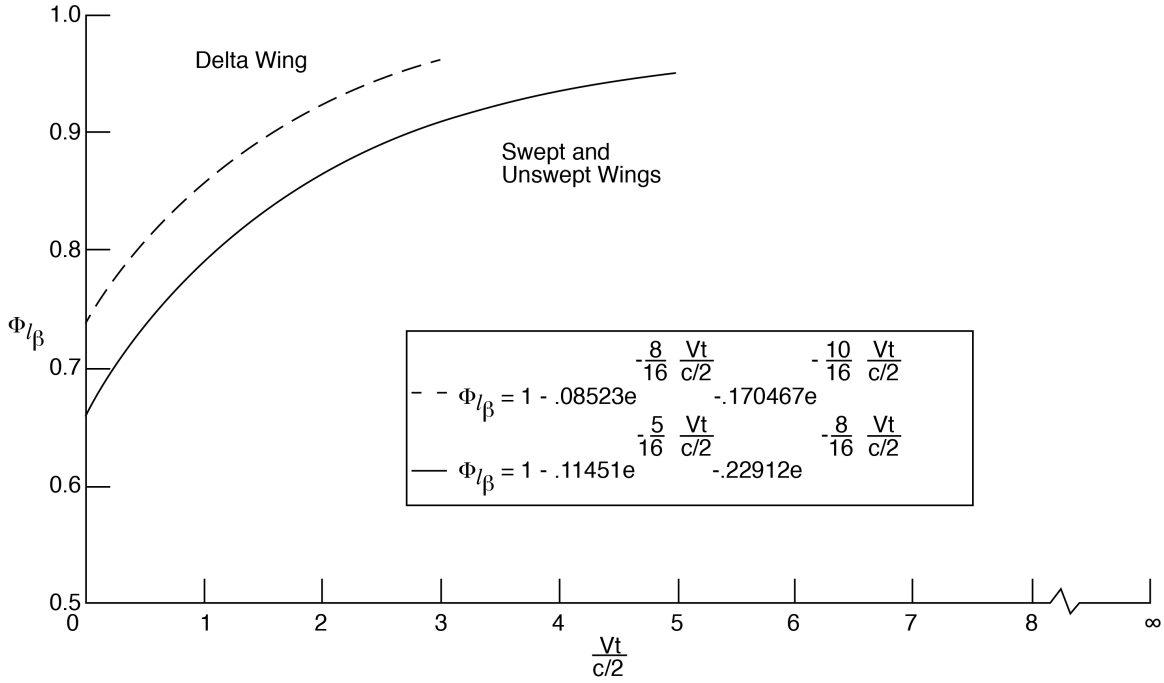

Figure 32. Indicial functions used for sideslip for three wings

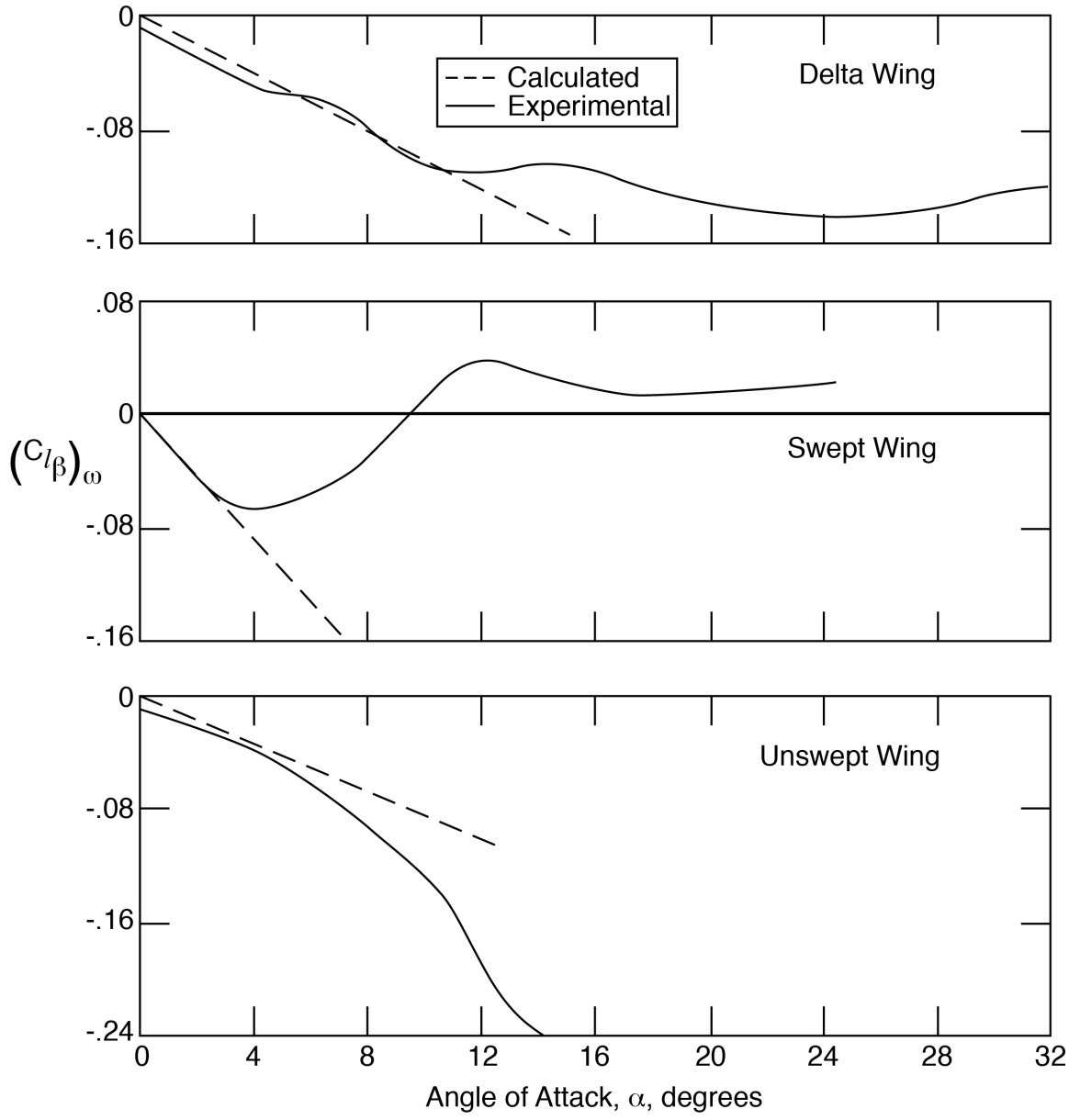

Figure 33. Comparison of calculated and experimental values for derivative $C_{l_{\beta,\omega}}$ for three wings (k_b = 0.22)

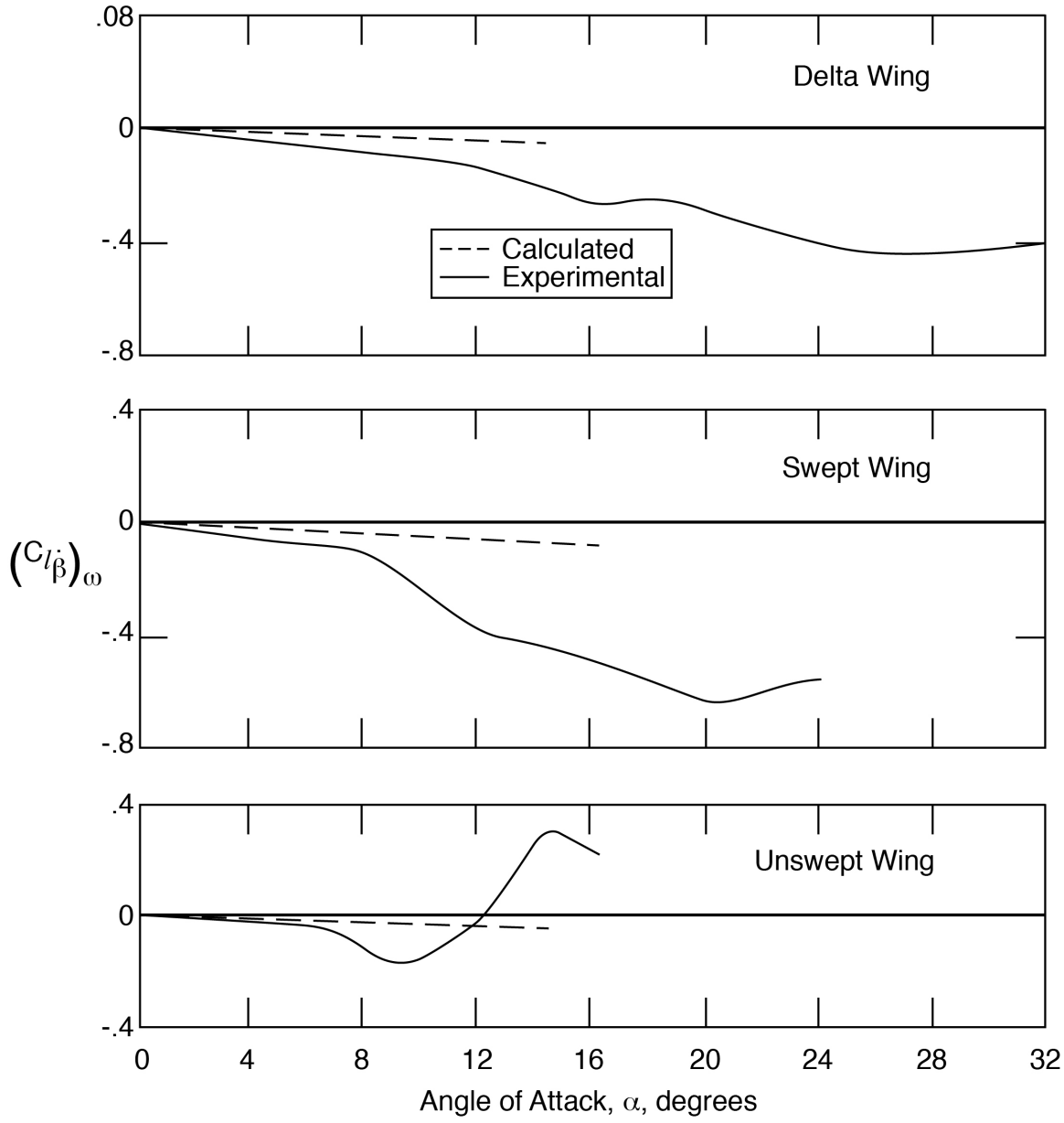

Figure 34. Comparison of calculated and experimental values for derivative $C_{l_{\dot{\beta},\omega}}$ for three wings (k_b = 0.22)

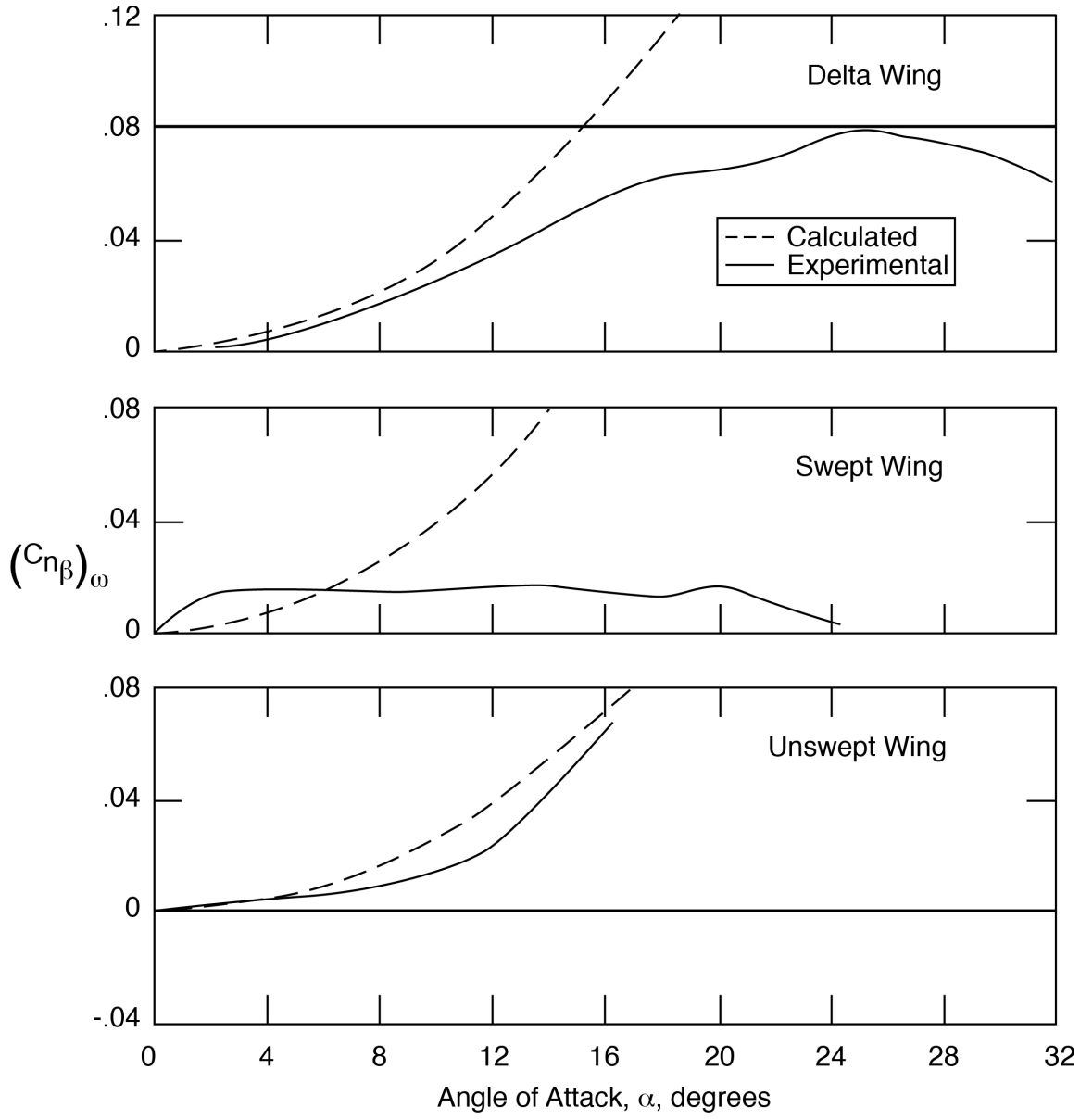

Figure 35. Comparison of calculated and experimental values for derivative $C_{n_{\beta,\omega}}$ for three wings (k_b = 0.22)

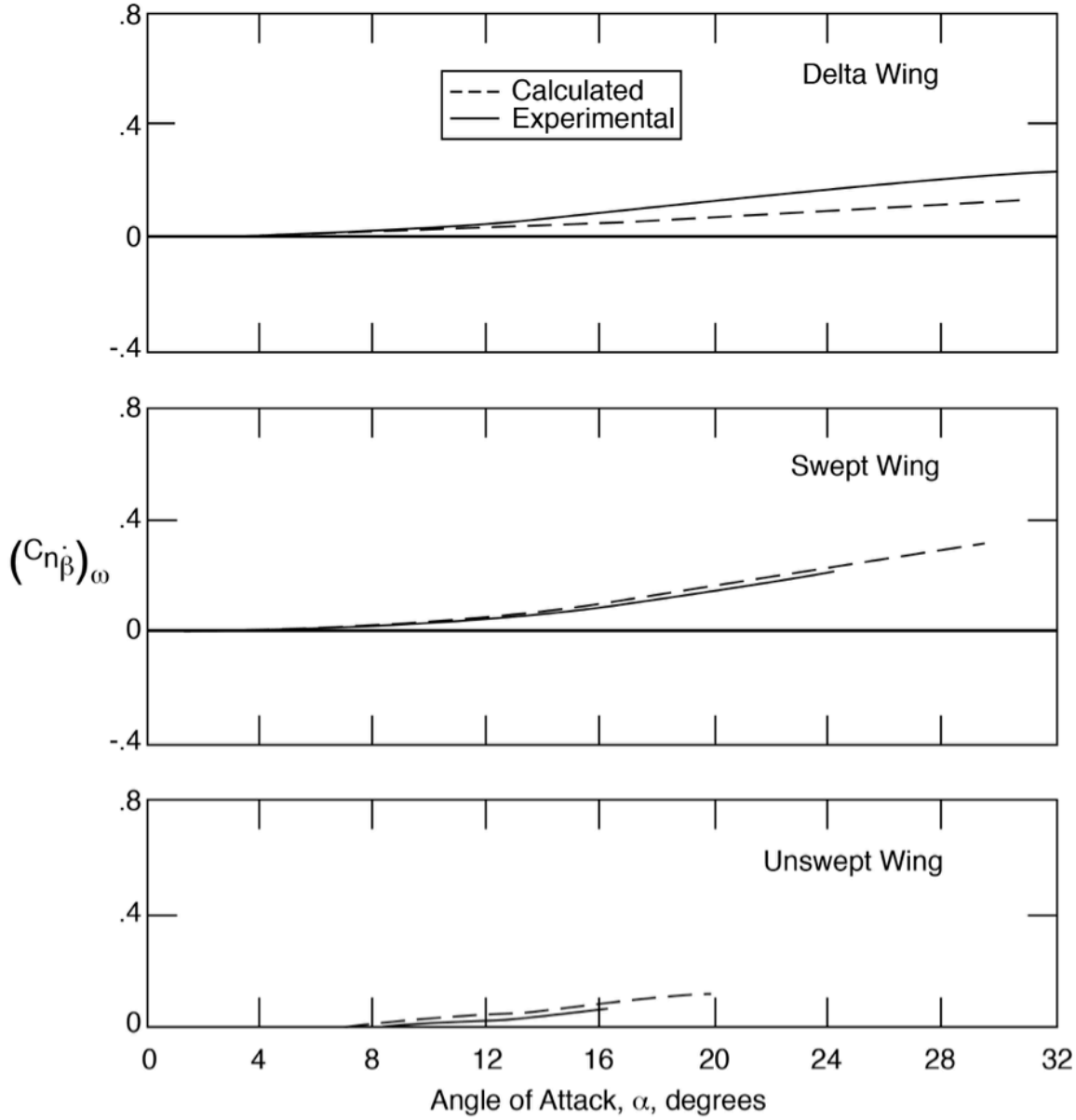

Figure 36. Comparison of calculated and experimental values for derivative $C_{n_{\dot{\beta},\omega}}$ for three wings (k_b = 0.22)

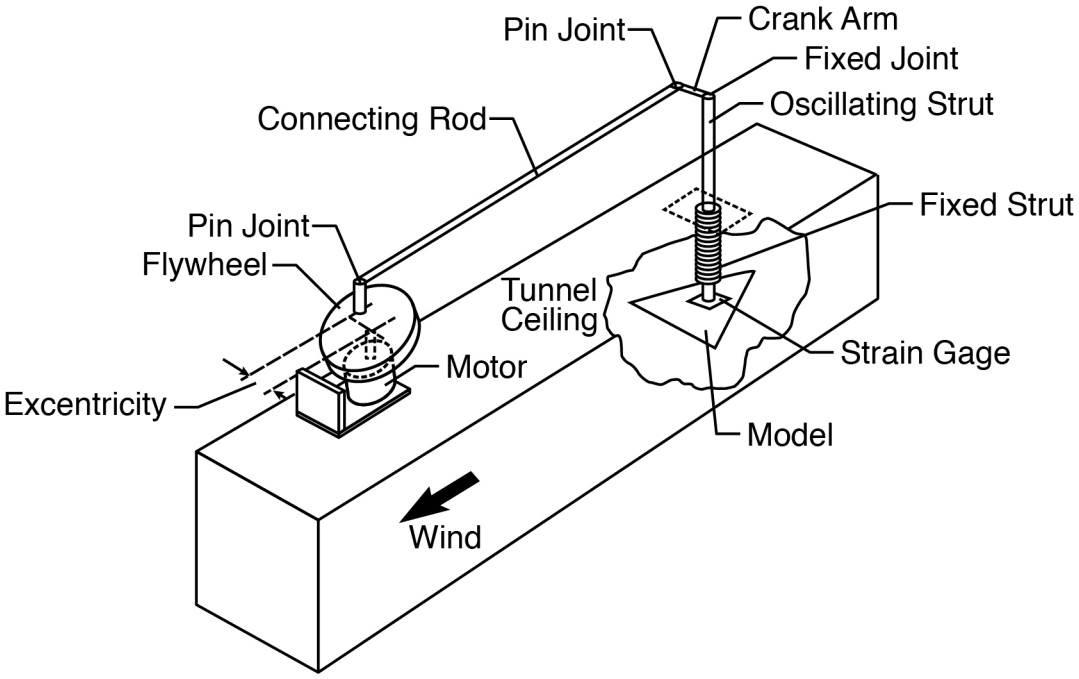

Figure 37. Sketch of oscillation-in-yaw equipment

Figure 38. Oscillation-in-yaw equipment installed on top of the Langley Stability Tunnel test section

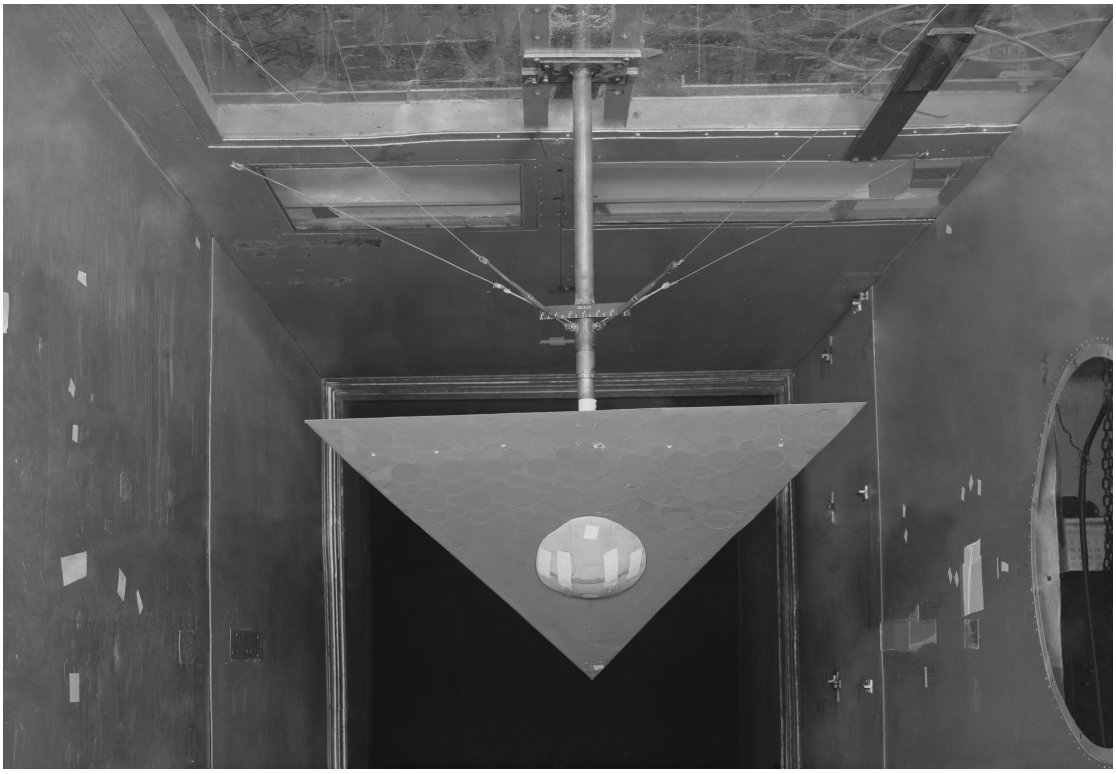

Figure 39a. Sixty-degree delta wing model on the vertical wind-axis yaw oscillation test rig in the Langley Stability Tunnel

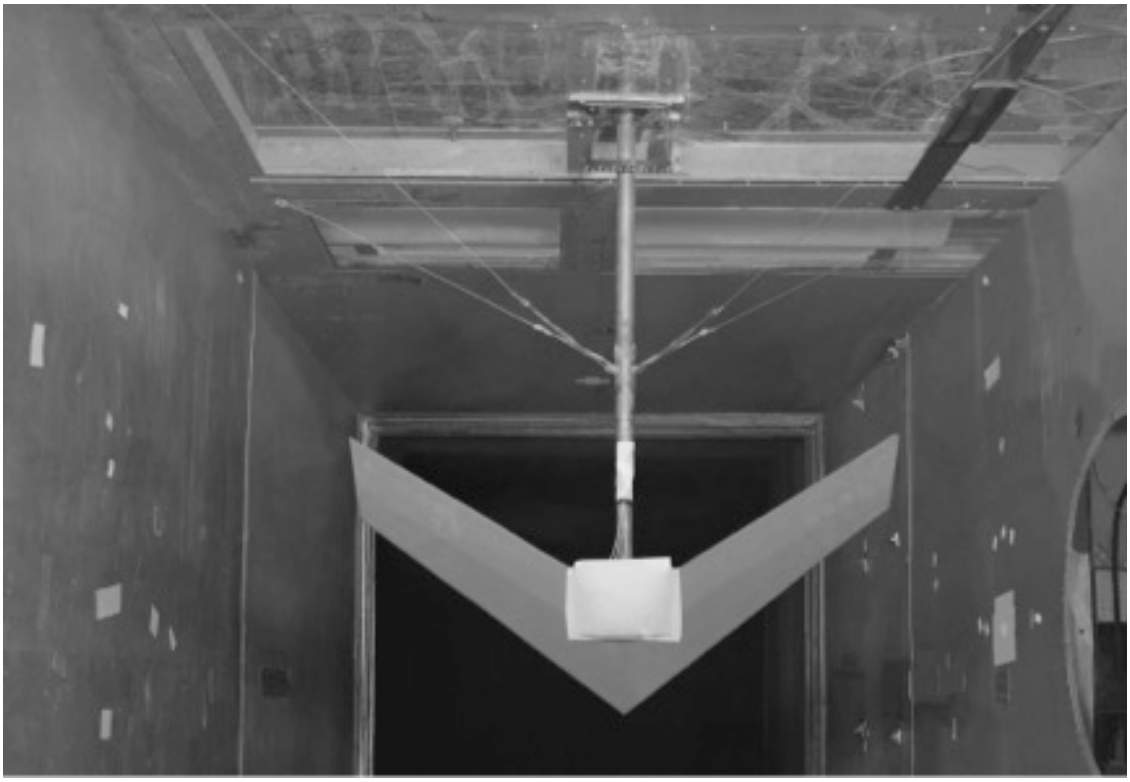

Figure 39b. Forty-five degree swept wing model on the vertical wind-axis yaw oscillation test rig in the Langley Stability Tunnel

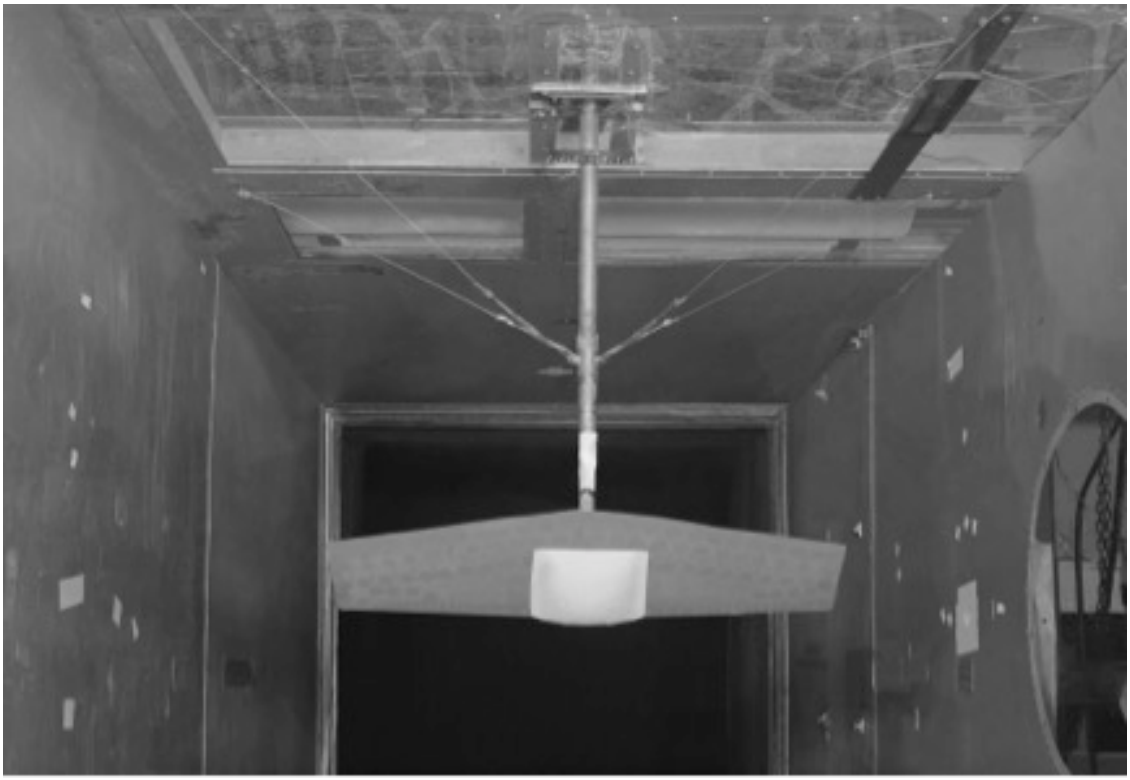

Figure 39c. Unswept wing model on the vertical wind-axis yaw oscillation test rig in the Langley Stability Tunnel

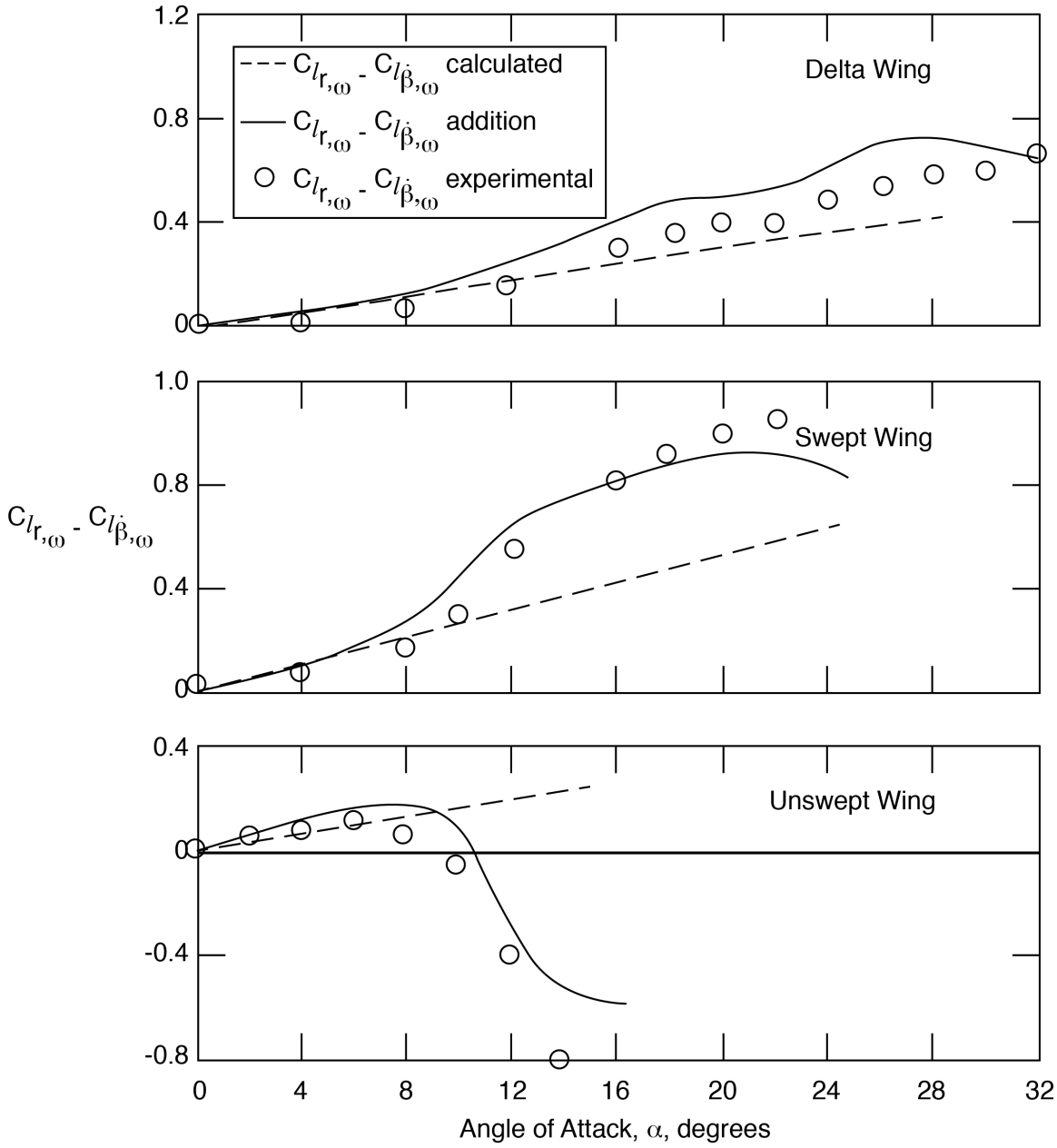

Figure 40. Comparison of calculated values with experimental measurements for the combination derivative $C_{l_{r,\omega}} - C_{l_{\dot{\beta},\omega}}$ ($k_b = 0.22$, Ψ ● 6° or 8°)

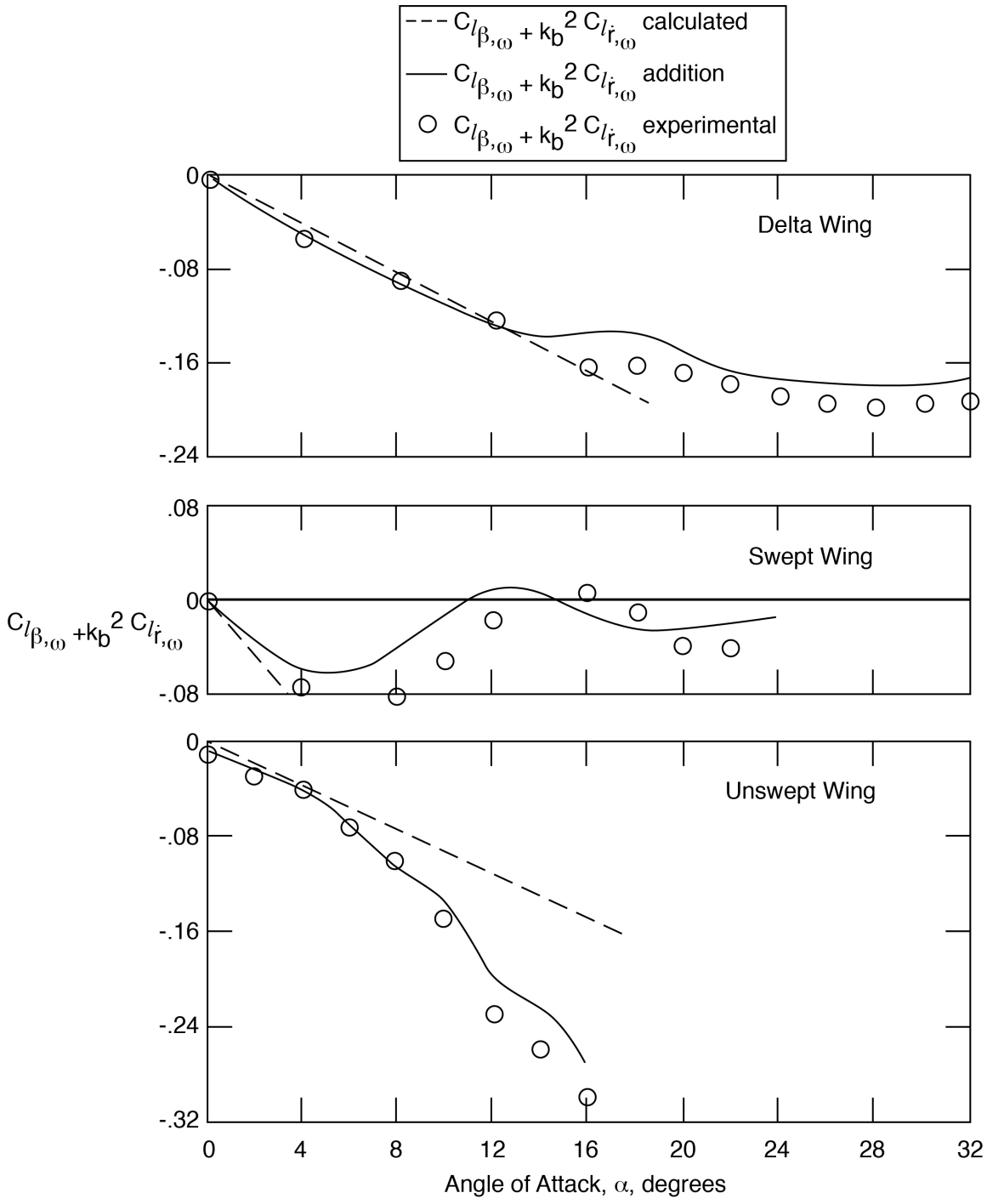

Figure 41. Comparison of calculated values with experimental measurements for the combination derivative $C_{l_{\beta,\omega}} + k_b^2 C_{l_{\dot{r},\omega}}$ ($k_b = 0.22$, Ψ ● 6° or 8°)

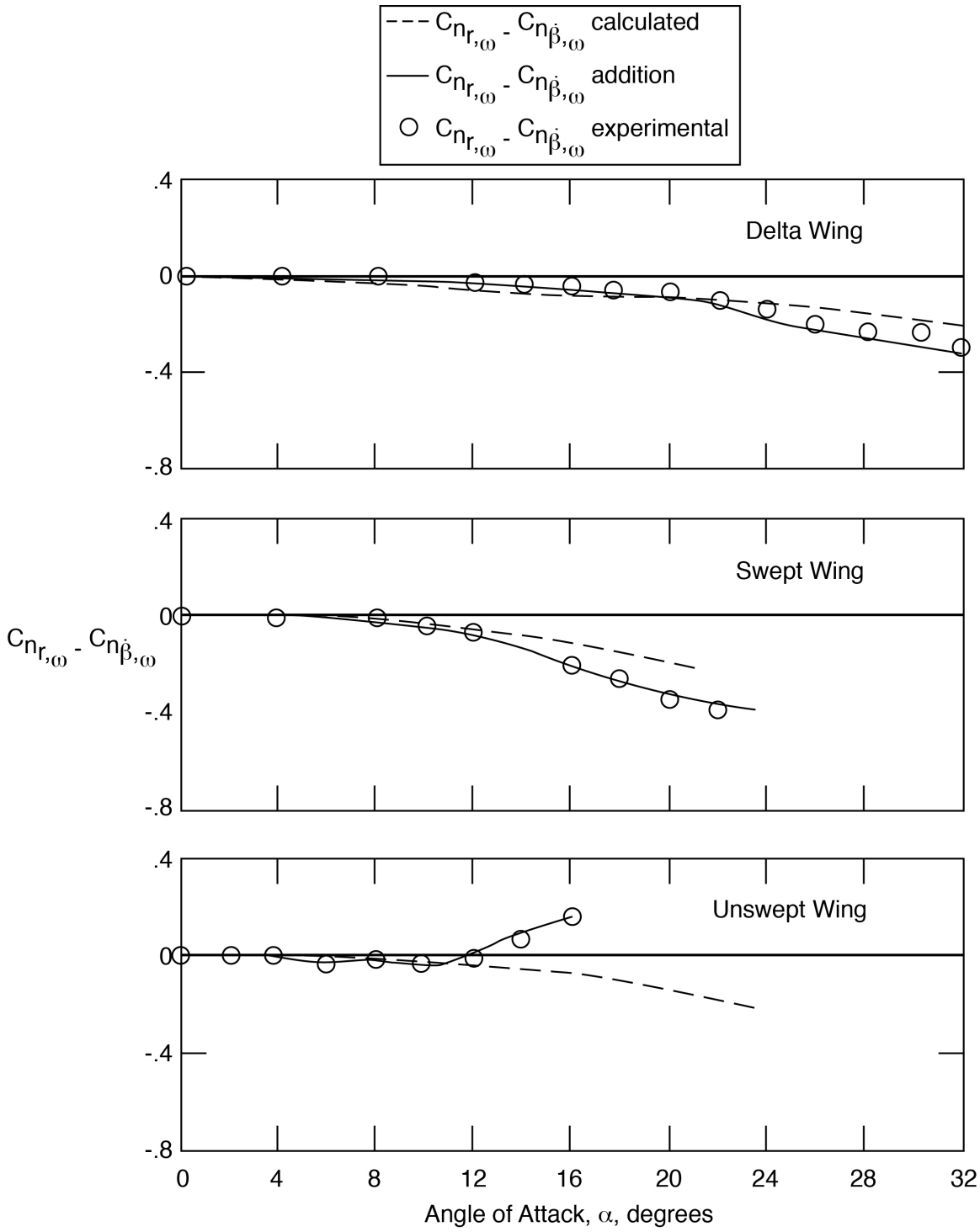

Figure 42. Comparison of calculated values with experimental measurements for the combination derivative $C_{n_{r,\omega}} - C_{n_{\dot{\beta},\omega}}$ ($k_b = 0.22$, Ψ ● 6° or 8°)

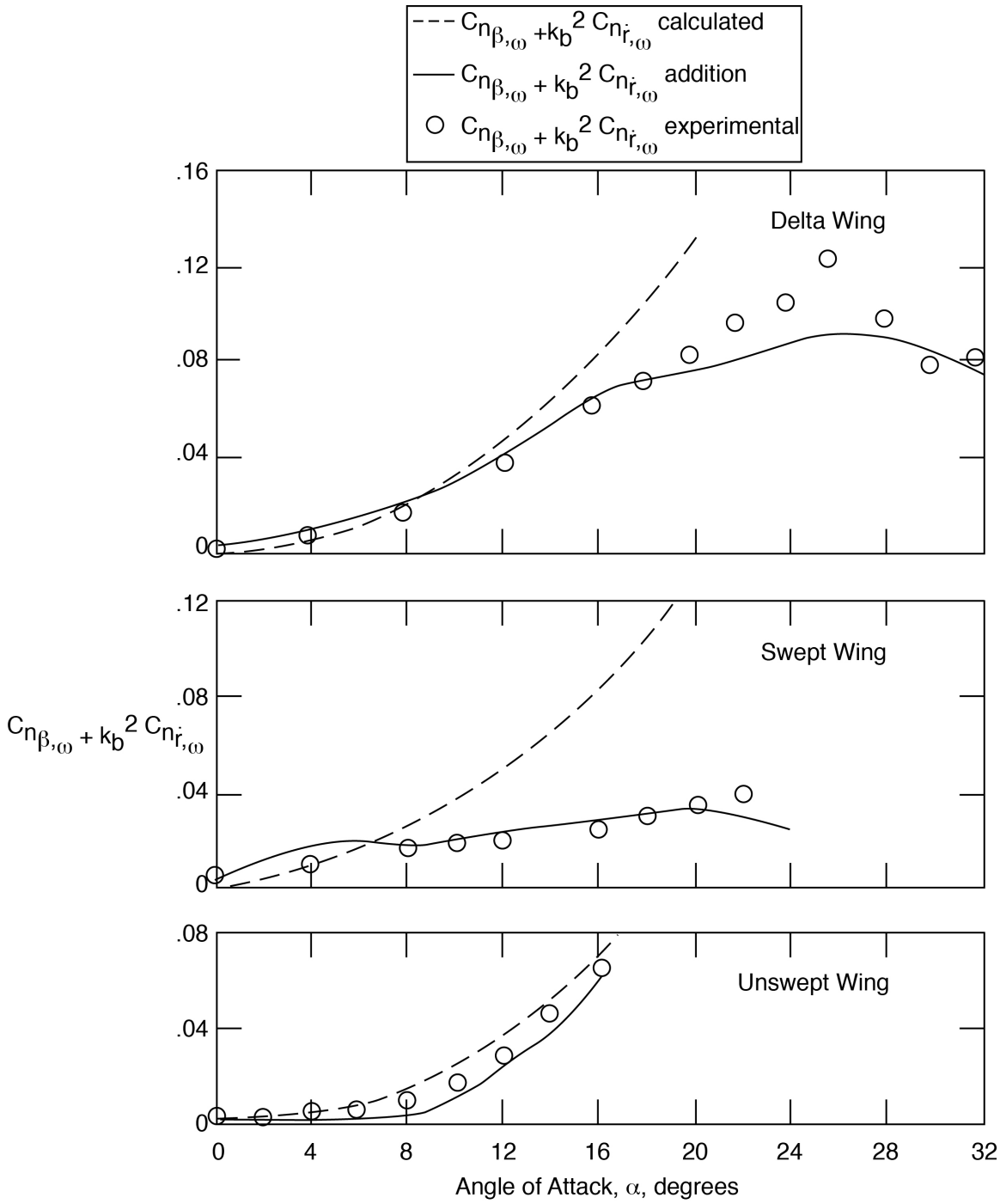

Figure 43. Comparison of calculated values with experimental measurements for the combination derivative $C_{n_{\beta,\omega}} + k_b^2 C_{n_{\dot{r},\omega}}$ (k_b = 0.22, Ψ ● 6° or 8°)

REPORT DOCUMENTATION PAGE

Form Approved
OMB No. 0704-0188

1. REPORT DATE *(DD-MM-YYYY)*	2. REPORT TYPE	3. DATES COVERED *(From - To)*
01- 12 - 2016	Technical Memorandum	

4. TITLE AND SUBTITLE

Calculated Low-Speed Steady and Time-Dependent Aerodynamic Derivatives for Several Different Wings Using a Discrete Vortex Method

5a. CONTRACT NUMBER

5b. GRANT NUMBER

5c. PROGRAM ELEMENT NUMBER

6. AUTHOR(S)

Riley, Donald R.

5d. PROJECT NUMBER

5e. TASK NUMBER

5f. WORK UNIT NUMBER

432938.11.01.07.43.40.17

7. PERFORMING ORGANIZATION NAME(S) AND ADDRESS(ES)

NASA Langley Research Center
Hampton, VA 23681-2199

8. PERFORMING ORGANIZATION REPORT NUMBER

L-20759

9. SPONSORING/MONITORING AGENCY NAME(S) AND ADDRESS(ES)

National Aeronautics and Space Administration
Washington, DC 20546-0001

10. SPONSOR/MONITOR'S ACRONYM(S)

NASA

11. SPONSOR/MONITOR'S REPORT NUMBER(S)

NASA-TM-2016-219349

12. DISTRIBUTION/AVAILABILITY STATEMENT

Unclassified - Unlimited
Subject Category 08
Availability: NASA STI Program (757) 864-9658

13. SUPPLEMENTARY NOTES

14. ABSTRACT

Calculated numerical values for some aerodynamic terms and stability Derivatives for several different wings in unseparated inviscid incompressible flow were made using a discrete vortex method involving a limited number of horseshoe vortices. Both longitudinal and lateral-directional derivatives were calculated for steady conditions as well as for sinusoidal oscillatory motions. Variables included the number of vortices used and the rotation axis/ moment center chordwise location. Frequencies considered were limited to the range of interest to vehicle dynamic stability (kb <.24). Comparisons of some calculated numerical results with experimental wind-tunnel measurements were in reasonable agreement in the low angle-of-attack range considering the differences existing between the mathematical representation and experimental wind-tunnel models tested. Of particular interest was the presence of induced drag for the oscillatory condition.

15. SUBJECT TERMS

Aerodynamic; Calculated; Derivatives; Discrete; Low-speed; Method; Steady; Time-dependent; Vortex; Wings

16. SECURITY CLASSIFICATION OF:			17. LIMITATION OF ABSTRACT	18. NUMBER OF PAGES	19a. NAME OF RESPONSIBLE PERSON
a. REPORT	b. ABSTRACT	c. THIS PAGE			STI Help Desk (email: help@sti.nasa.gov)
U	U	U	UU	67	19b. TELEPHONE NUMBER *(Include area code)* (757) 864-9658